

Article

Structural Assessment Based on Vibration Measurement Test Combined with an Artificial Neural Network for the Steel Truss Bridge

Minh Q. Tran ¹, Helder S. Sousa ¹ , Thuc V. Ngo ² , Binh D. Nguyen ¹, Quyen T. Nguyen ³ , Huan X. Nguyen ⁴, Edward Baron ¹ , José Matos ¹  and Son N. Dang ^{1,*} 

¹ ISISE, ARISE, Department of Civil Engineering, University of Minho, 4800-058 Guimarães, Portugal

² Institute of Science and International Cooperation, Mien Tay Construction University, Vinh Long 85100, Vietnam

³ 2C2T-Centro de Ciência e Tecnologia Têxtil, Universidade do Minho, 4800-058 Guimarães, Portugal

⁴ Faculty of Science and Technology, Middlesex University, London NW4 4BT, UK

* Correspondence: sondn@civil.uminho.pt

Abstract: Damage assessment is one of the most crucial issues for bridge engineers during the operational and maintenance phase, especially for existing steel bridges. Among several methodologies, the vibration measurement test is a typical approach, in which the natural frequency variation of the structure is monitored to detect the existence of damage. However, locating and quantifying the damage is still a big challenge for this method, due to the required human resources and logistics involved. In this regard, an artificial intelligence (AI)-based approach seems to be a potential way of overcoming such obstacles. This study deployed a comprehensive campaign to determine all the dynamic parameters of a predamaged steel truss bridge structure. Based on the results for mode shape, natural frequency, and damping ratio, a finite element model (FEM) was created and updated. The artificial intelligence network's input data from the damage cases were then analysed and evaluated. The trained artificial neural network model was curated and evaluated to confirm the approach's feasibility. During the actual operational stage of the steel truss bridge, this damage assessment system showed good performance, in terms of monitoring the structural behaviour of the bridge under some unexpected accidents.

Keywords: ANN; FEM; damage assessment; structural health monitoring; steel truss bridge



Citation: Tran, M.Q.; Sousa, H.S.; Ngo, T.V.; Nguyen, B.D.; Nguyen, Q.T.; Nguyen, H.X.; Baron, E.; Matos, J.; Dang, S.N. Structural Assessment Based on Vibration Measurement Test Combined with an Artificial Neural Network for the Steel Truss Bridge. *Appl. Sci.* **2023**, *13*, 7484. <https://doi.org/10.3390/app13137484>

Academic Editor: Mahmoud Bayat

Received: 30 May 2023

Revised: 14 June 2023

Accepted: 18 June 2023

Published: 25 June 2023



Copyright: © 2023 by the authors. Licensee MDPI, Basel, Switzerland. This article is an open access article distributed under the terms and conditions of the Creative Commons Attribution (CC BY) license (<https://creativecommons.org/licenses/by/4.0/>).

1. Introduction

The regular monitoring and assessment of a bridge's structural behaviour is essential for the early detection of construction defects. It enables the maintenance and repair of the system at an early stage, ensuring the safety and reliability of the structure at a minimal cost. Decades ago, visual inspection was the most common method of detecting structural damage. However, visual inspection solutions are often quite laborious and time-consuming, which consumes high costs for workers and assessors, with a low overall efficiency. This is especially true when structural dismantling (e.g., cutting, taking samples, among others) is required to access the area to be tested; these have the effect of changing the physical properties, and can thus reduce the structure's bearing capacity. In addition, visual inspection techniques can only help identify damage that is visible on the structure's surface. For large and complex structures (such as cable-stayed bridges and suspension bridges), the visual inspection method is challenging to use, and is therefore no longer suitable.

In the past, when sensor technology had not yet been developed, structural health monitoring was often performed based on geodetic engineering and machinery [1–4]. Structural health monitoring is based on the characteristics of geometrical factors, such as settlement, deformation, and displacement. In this regard, creating a coordinate system

according to the country's coordinate grid is necessary. On the other hand, these coordinate systems should meet the technical requirements specified by the national standards. The observations can then be made at the predetermined locations, and compared with the first measurement. The results are then processed and evaluated by experts, in accordance with national specifications. However, this approach still retains many disadvantages; both the cost of creating a coordinate system and the cost for the experts are expensive. In addition, the results cannot detect damage inside the structure, and only when large movements occur will there be warnings of the need to repair the bridges [5,6].

Most structural health monitoring solutions are based on assessing the structure's response to external stimuli. Based on this, several static testing methods have been implemented. Several researchers have used and implemented static data in their studies for damage detection [7–12]. The principle is to use loads equal to or less than the design loads, such that they act on the structure. Information about the displacement and deformation at dangerous locations (or locations that need to be determined) can then be accurately identified. This method is intuitive, easy to understand, and highly reliable. However, logistics work requires a lot of money; some equipment is expensive, or can only be used once for a position (e.g., strain gauge). This method also has the disadvantage of necessitating the suspension of traffic from utilising the bridge during the experiment. This causes difficulties for bridges on important traffic routes with high traffic density, or bridges located in cities.

To overcome the disadvantages of the visual inspection method, as well as the static test method, non-destructive structural damage detection techniques have been developed. Non-destructive health monitoring techniques can be classified as either global methods or local methods. Local methods focus on only part of the structure, and include ultrasonic or acoustic methods, magnet field methods, X-ray inspection. However, these methods, by merit of being local approaches, require prior information about the location of the damaged area [13]. One of the methods for monitoring global structural health is based on vibration measurements. Accordingly, it is more effective to use dynamic responses, such as degradation detection, to detect both abrupt and gradual changes. The dynamic measurement of responses requires the control of both environmental and operational impacts, in order to achieve accurate data. In previous studies, dynamic-based methods have been based on frequency measurements. This is mainly due to the higher accuracy of frequency-measuring instruments when compared to geometrical or mode-measuring instruments. With the subsequent advancement of such instrumentation, vibration-based methods have also been considered. In this regard, we propose damage assessment using either natural frequency [14], or from the parameters of the vibration characteristics [15].

The potential of applying vibration-based methods to a real-life bridge is an attractive prospect, and significant attention is being paid to it by many researchers [16–20]. Numerous variables, such as the weather, the wind, the amount of traffic, and data quality (signal-to-noise ratio), have an impact on this methodological approach. The use of natural frequency, mode shape, mode shape curvature, and dynamically measured flexibility has led to the identification of several different vibration-based approaches. These methods appeared during the late 1970s, examining the significance of statistics for vibration-based methods applied on forty highway bridges in New Mexico [21,22]. Since then, various parts of these vibration-based techniques have been researched, using experimental data collected from existing bridges [23,24]. The vibration data collection techniques have also been researched and developed. The two main groups of methods that have been used are direct vibration measurement and indirect vibration measurement [25].

Only monitoring the change in frequency stops at determining the mere occurrence of damage [26–28]. Several similar applications have been introduced, as follows: a method of analysing natural frequencies of beam structures with some random cracks based on the transfer matrix method and a rotational spring model of cracks [29]; using a vector of the first natural frequencies as the multivariable input damage determination on two real works [30]; using the natural frequency of the texture to determine the existence

of damage [31–38]. However, these approaches require preliminary tests to determine the natural frequency of the structure before failure occurs. For aged structure, without data, this is very difficult to achieve. In addition, few researchers have applied natural frequency to such complex structures as spatial frame bridges. Furthermore, another disadvantage of this method is that natural frequency information is impractical, because some combinations of failure phenomena (such as cracks at different locations) can produce similar changes in natural frequency.

Along with the contemporary development of information technology, artificial intelligence and machine learning attempt to bring computers a little closer to the brain's capabilities, using a highly simplified imitation of some components of information processing in the brain. These neural networks study the human brain's capabilities and imitates them in hardware, software, or other devices. Once trained, the neural network can identify similarities in fresh input patterns and predict the output pattern as a result. The learning process and the testing process are the two fundamental functions of a neural network. Learning is the process of gaining knowledge from pre-existing information. This procedure has three steps: computing the output, comparing it to the intended target, and adjusting the weight. This procedure is then repeated for the metrics sample data set. A target function or a function error expresses the quality of the learning process.

In recent years, interest has risen in using AI and machine learning in SHM [39]. In a lot of research, methods for detecting damage in beams and bridges have been combined with machine learning and vibration-based damage-detection techniques [40,41]. In this regard, several algorithms have also been introduced, as follows: the particle swarm optimisation (PSO) algorithm, in combination with the use of modal data to determine the damage in the structures, including two beam structures and two truss structures [42]; the Genetic Algorithm (GA), applying residual force methods based on the theory of specific vibration analysis to identify failures in elastic structures [43]; combining a strain energy-based index with PSO to determine the location and extent of various failures [44]; Ant colony optimisation (AC), applied to determine the damage location of the 2-story frame and 3-story steel frame structures corrected on measurements [45]; a combined GA algorithm and information synthesis technique, to determine the location and extent of damage at many locations in the structure [46]; a GA algorithm, to detect damage in frames and cantilever beams using an objective function, including natural frequency, mode shapes, and both [47]; and finally, using both the GA and dynamic characteristics of the structure [48]. These applications demonstrated the potential of combining artificial intelligence and vibration-based methods in SHM, but were mostly performed on small, simple structures.

With a huge structure, operation and maintenance often consume a lot of resources. Solutions for visual monitoring or static load testing significantly increase maintenance costs. It would also be extremely costly to make too many measurements of the overall vibration of the structure. This study has presented and tested a comprehensive solution on an actual steel truss bridge. To determine and quantify the damage from the steel truss bridge, efforts were made to combine artificial neural network and vibration measurement results. Hopefully, this solution can help engineers to save time, resources, and cost.

2. Theoretical Approach

2.1. Using Dynamic Features to Detect Damage

Considering a finite structure of degrees of freedom, the structure's partial vibration differential equation has the following form [49]:

$$M\ddot{u}(t) + Ku(t) = 0 \quad (1)$$

for which:

M = structure's mass matrix;

K = structure's stiffness matrix.

The equations of the vibration of the masses have the form:

$$u_i(t) = A_i \sin(\omega t + \varphi_i) \tag{2}$$

$$\ddot{u}_i(t) = -\omega^2 A_i \sin(\omega t + \varphi_i) \tag{3}$$

The equations and components can then be substituted into Equation (1):

$$\begin{bmatrix} m_1 & & & \\ & m_2 & & \\ & & \dots & \\ & & & m_n \end{bmatrix} (-\omega^2) \begin{bmatrix} A_1 \\ A_2 \\ \dots \\ A_n \end{bmatrix} + \begin{bmatrix} k_{11} & k_{12} & \dots & k_{1n} \\ k_{21} & k_{22} & \dots & k_{2n} \\ \dots & \dots & \dots & \dots \\ k_{n1} & k_{n2} & \dots & k_{nn} \end{bmatrix} \begin{bmatrix} A_1 \\ A_2 \\ \dots \\ A_n \end{bmatrix} = 0 \tag{4}$$

or

$$\left[\begin{bmatrix} k_{11} & k_{12} & \dots & k_{1n} \\ k_{21} & k_{22} & \dots & k_{2n} \\ \dots & \dots & \dots & \dots \\ k_{n1} & k_{n2} & \dots & k_{nn} \end{bmatrix} - \omega^2 \begin{bmatrix} m_1 & & & \\ & m_2 & & \\ & & \dots & \\ & & & m_n \end{bmatrix} \right] \begin{bmatrix} 1 \\ \varphi_2 \\ \dots \\ \varphi_n \end{bmatrix} = 0 \tag{5}$$

To obtain the equation for determining the specific type of vibration, this can then be simplified:

$$[\mathbf{K} - \omega_j^2 \mathbf{M}] \phi_j = 0 \tag{6}$$

Natural frequency ($f = \omega/2\pi$) and natural vibration mode shape (φ_i), determined through Equation (5) or Equation (6), are very important features of the structure. The dynamic characteristic is unique to a particular structure. With Equations (1)–(6), the modal properties of the structure (i.e., the frequencies and mode shapes, damping ratio, among others) at both an intact and damaged state are extracted.

2.2. Artificial Neural Network

The Artificial Neural Network (ANN) was inspired and developed based on the human nervous system. The ability of ANN to gain knowledge from experience and enhance performance is one of its hallmark characteristics. Recognition, control systems, classification, pattern recognition, and image processing are a few examples of ANN applications. The input layer, hidden layer, and output layer are the three primary parts of an ANN. At each layer, neurons form nodes, which then act as data kernels. The neurons are connected to each other through the associations created using the training parameter (weight and bias). The processing element is connected at each node (or neuron) to synapses, according to neuron’s number in the previous processing layer.

The signalling between neurons in layers is depicted in Figure 1. After receiving input samples, the input layer sends the signal to the hidden layer. The input and output layers are connected with a certain number of neurons in the hidden layer. The connections between each neuron in the previous layers and the subsequent layers depend on the training parameters (weight and bias). Summation and activation functions serve as the foundation for signal transmission.

The summation function is calculated from the input layer to the hidden layer as the bias, weight ratios, and output signals of the preceding layers (Equation (7)), as follows:

$$\sum_{i_2}^1 = \sum_{i_1, i_2}^{n_1, n_2} w_{i_1 i_2}^1 \times f_{i_1} + w_{i_2}^1; i_1 = (1 : n_1); i_2 = (1 : n_2) \tag{7}$$

in which $w_{i_1 i_2}^1$ is the weight coefficients, $w_{i_2}^1$ is the bias coefficients; f_{i_1} indicates the input data of the i_1 neuron; n_1 and n_2 are the number of neurons in the input layer and the hidden layer; and $\sum_{i_2}^1$ denotes the input of the i_2 neuron of the hidden layer.

The activation function is used to restrict the output’s value range in the next step. The activation function may be either linearly or nonlinearly monotonically increasing. There are many types of activation functions that have been studied: threshold function, rectified linear unit function (ReLU), sigmoid function, hyperbolic tangent function, and softmax function, etc. In this study, a sigmoid activation function was used to address nonlinear issues (Equation (8)).

$$O_{i_2} = \frac{1}{1 + e^{-\Sigma_{i_2}^1}} \tag{8}$$

The processing and transmission for the hidden and output layers were handled in the same way as they were for the input and hidden layers. Equations (8) and (9) illustrate this process:

$$\Sigma_{i_3}^2 = \sum_{i_2, i_3}^{n_2, n_3} w_{i_2 i_3}^2 \times O_{i_2} + w_{i_3}^2; i_3 = (1 : n_3) \tag{9}$$

$\Sigma_{i_3}^2$ represents i_3 ’s input neuron, and n_3 is the output layer’s neuron.

$$O_{i_3} = \frac{1}{1 + e^{-\Sigma_{i_3}^2}} \tag{10}$$

Then, the difference between the predicted result and the real output was calculated:

$$\chi(w) = \sum_{k=1}^{N_k} \frac{1}{2} \frac{(O_{i_3}^k - \bar{O}_{i_3}^k)^2}{N_k} \tag{11}$$

$O_{i_3}^k$ and $\bar{O}_{i_3}^k$ are the predicted output and the actual output of the k th output data, respectively, and N_k is the quantity of output data. The goal of the network was to minimise the difference between the prediction and real output $\chi(w)$. The training parameters were transferred, so as to apply the reverse process based on the Gradient descent techniques (GD):

$$\frac{\partial \Sigma_{i_3}^2}{\partial w_{i_2 i_3}^2} \times \frac{\partial O_{i_3}}{\partial \Sigma_{i_3}^2} \times \frac{\partial \chi(w)}{\partial O_{i_3}} = \frac{\partial \chi(w)}{\partial w_{i_2 i_3}^2} \tag{12}$$

$$\frac{\partial \Sigma_{i_3}^2}{\partial w_{i_3}^2} \times \frac{\partial O_{i_3}}{\partial \Sigma_{i_3}^2} \times \frac{\partial \chi(w)}{\partial O_{i_3}} = \frac{\partial \chi(w)}{\partial w_{i_3}^2} \tag{13}$$

$$\frac{\partial \Sigma_{i_3}^2}{\partial w_{i_2 i_3}^2} = O_{i_2}; \frac{\partial O_{i_3}}{\partial \Sigma_{i_3}^2} = \frac{e^{-\Sigma_{i_3}^2}}{(1 + e^{-\Sigma_{i_3}^2})^2} \tag{14}$$

$$\frac{\partial \chi(w)}{\partial O_{i_3}} = (O_{i_3}^k - \bar{O}_{i_3}^k) \tag{15}$$

$$\frac{\partial \Sigma_{i_3}^2}{\partial w_{i_3}^2} = 1 \tag{16}$$

$$\frac{\partial O_{i_3}}{\partial \Sigma_{i_3}^2} = \frac{e^{-\Sigma_{i_3}^2}}{(1 + e^{-\Sigma_{i_3}^2})^2} \tag{17}$$

New training parameters connecting classes were obtained according to the following equations:

$$w_{i_2 i_3}^2 + = w_{i_2 i_3}^2 - \frac{\tau \times \partial \chi(w)}{\partial w_{i_2 i_3}^2} \tag{18}$$

$$w_{i_3}^{2+} = w_{i_3}^2 - \frac{\tau \times \partial\chi(w)}{\partial w_{i_3}^2} \tag{19}$$

$$\frac{\partial \Sigma_{i_2}^1}{\partial w_{i_1 i_2}^1} \times \frac{\partial O_{i_2}}{\partial \Sigma_{i_2}^1} \times \frac{\partial \chi(w)}{\partial O_{i_2}} = \frac{\partial \chi(w)}{\partial w_{i_1 i_2}^1} \tag{20}$$

$$\frac{\partial \Sigma_{i_2}^1}{\partial w_{i_2}^1} \times \frac{\partial O_{i_2}}{\partial \Sigma_{i_2}^1} \times \frac{\partial \chi(w)}{\partial O_{i_2}} = \frac{\partial \chi(w)}{\partial w_{i_2}^1} \tag{21}$$

$$\frac{\partial \Sigma_{i_2}^1}{\partial w_{i_1 i_2}^1} = f_{i_1}; \frac{\partial O_{i_2}}{\partial \Sigma_{i_2}^1} = \frac{e^{-\Sigma_{i_2}^1}}{(1 + e^{-\Sigma_{i_2}^1})^2} \tag{22}$$

$$\frac{\partial \Sigma_{i_2}^1}{\partial w_{i_2}^1} = 1 \tag{23}$$

$$w_{i_1 i_2}^{1+} = w_{i_1 i_2}^1 - \frac{\tau \times \partial\chi(w)}{\partial w_{i_1 i_2}^1} \tag{24}$$

$$w_{i_2}^{1+} = w_{i_2}^1 - \frac{\tau \times \partial\chi(w)}{\partial w_{i_2}^1} \tag{25}$$

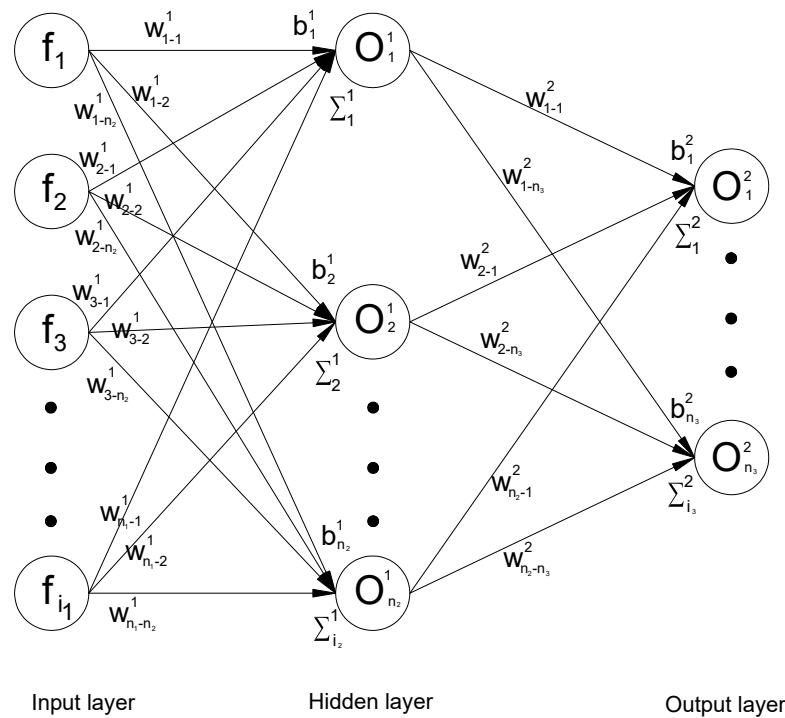


Figure 1. Architecture for artificial neural networks.

The Equations (7)–(25) [50–52] were used to iteratively train the neural network. When the goal or the maximum number of loops was attained, the iteration came to an end.

In this study, a comprehensive campaign of experimental measurements of the dynamic characteristics were carried out. Natural frequency and mode shape were identified as two dynamic properties of the structure. The results from the measurement experiment were used to update the numerical model. This model would thus have the least deviation from reality. With the updated model, the damage scenarios have been calculated and given as data to train the ANN.

3. Case Study

3.1. Chuong Duong Bridge Introduction

Chuong Duong Bridge (Figure 2) was one of the first large bridges to be built in Hanoi, Vietnam. The bridge was built in the period 1983 to 1985. Chuong Duong bridge connected the Hoan Kiem district to the Long Bien district, with a total length of 1230 m (from the abutment on the Hoan Kiem side to the abutment on the Long Bien side). The main bridge is a steel truss bridge, comprising 11 spans with the following measurements: 88 m + 92 m + 89.94 m + 89.28 m \times 7 + 84.88 m. Of these, the three spans in the Hoan Kiem district (88 m + 92 m + 89.94 m) are continuous structures, while the other spans are simple steel trusses.



Figure 2. Chuong Duong bridge.

The entire width of the bridge is 20.06 m (Figure 3). The bridge carries a four-lane road: two lanes in the middle for cars and buses, with the other two reserved for motorcycles. The bridge is designed with a load of H-30 on the main lane and H-6 on both sides of the cantilever. In the first days of being put into operation, this bridge had a traffic turnover of 7000–8000 vehicles per day. However, the number of vehicles crossing the bridge has since increased dramatically, now reaching tens of thousands of vehicles per day.

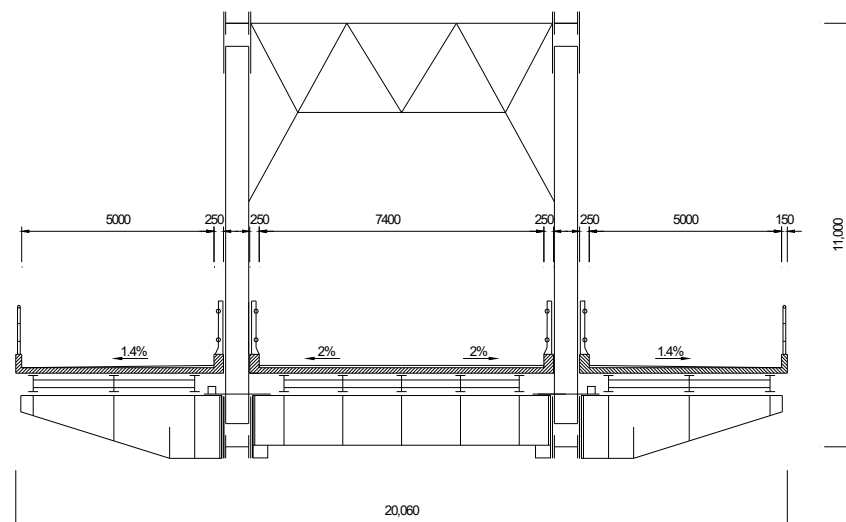


Figure 3. Detailed cross section of Chuong Duong bridge.

The main truss rods have an H-shaped cross-section, whose height depends on their position (see Table 4 for the details). At the truss nodes, a 32 mm thick panel is used to connect the truss ends.

3.2. On-Site Measurement Campaign before Damage

3.2.1. Description of Experiment

In the framework of this study, a comprehensive survey and measurement campaign was carried out on Span 8 of the Chuong Duong bridge. The campaign included geometric surveys and vibration measurements of the entirety of Span 8. After finishing the geometric survey, we conducted vibration measurements under random stimuli (wind, current, surrounding loads, vehicles crossing the bridge, among others). Eight highly sensitive sensors, ranging in sensitivity from 1054 to 1083 mV/m/s², were used. With a sampling frequency of 1651 Hz, each setup's average acquisition time was 30 min. To achieve the vibration modes of the entire span, a measuring grid of 34 points (covering all truss nodes) was established (Figure 4).

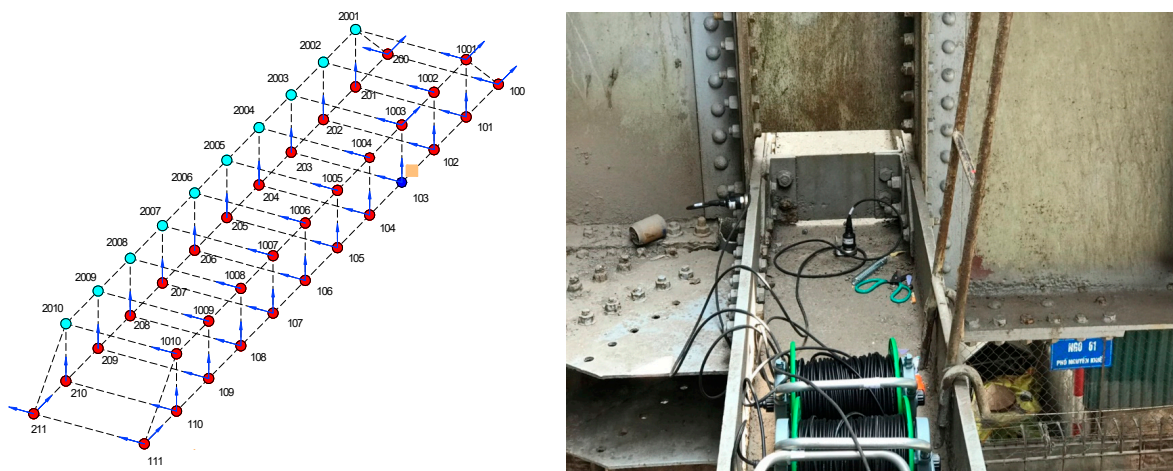


Figure 4. Placement of measurement points on Span 8 of the Chuong Duong bridge (blue: reference point, red: moving points, in addition to the sensor installation position at the truss node).

However, due to the limited number of sensors (of which there were eight), the measuring grid has been divided into eight setups. The reference point at node 103 has been selected to link the data from the sensors. Other moving points were located at truss nodes on the bridge (Figure 5). All points defined in the overall measurement grid would thus be fully covered using these setups.

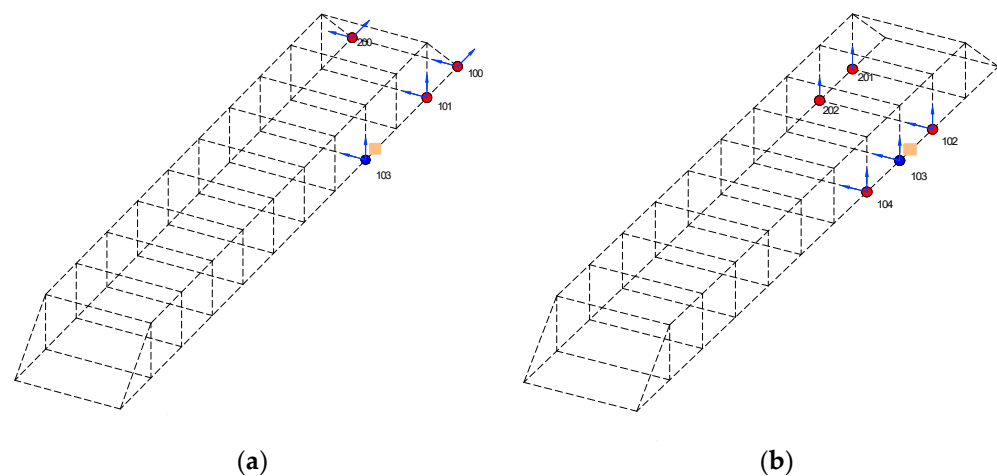


Figure 5. Cont.

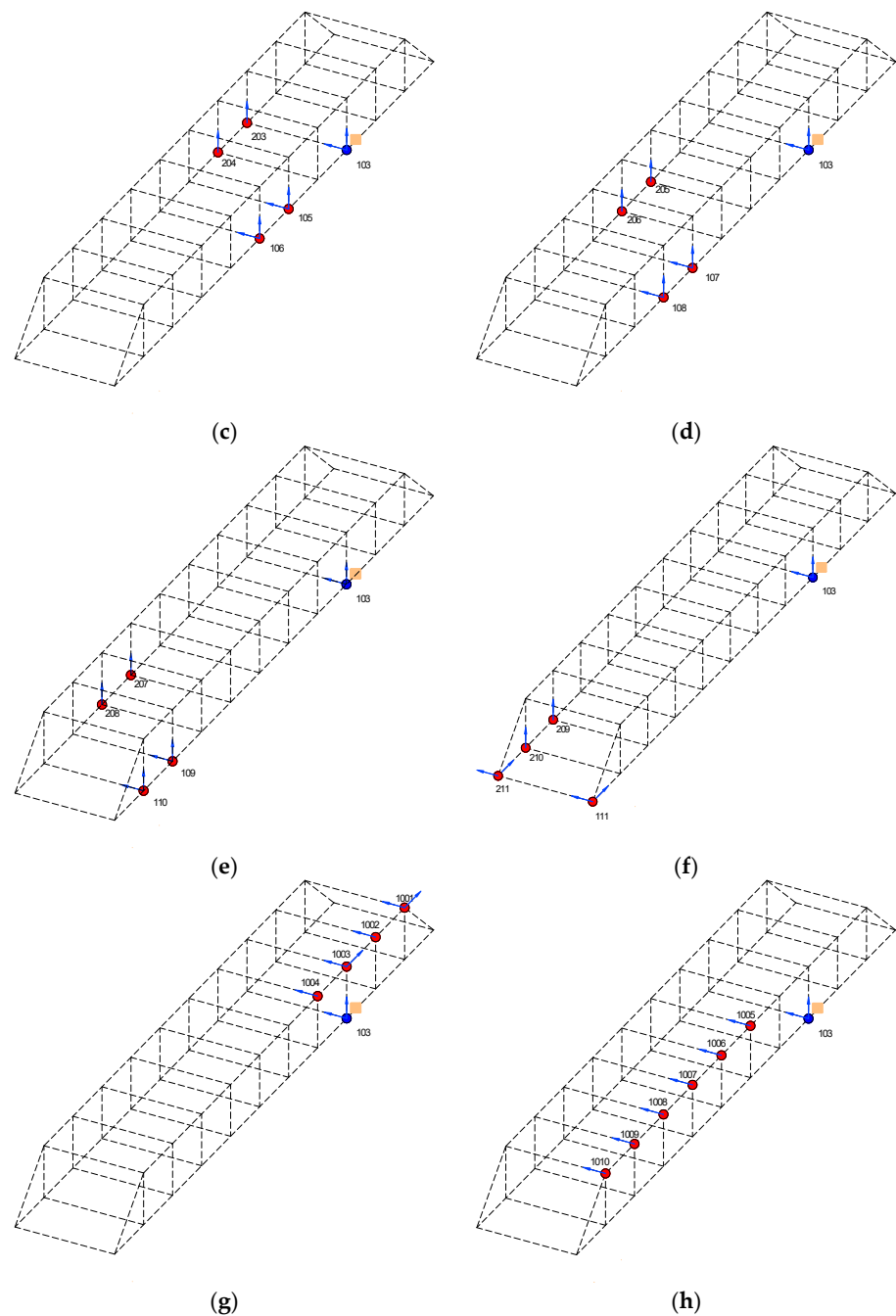


Figure 5. The measurement setups: (a) Setup 1; (b) Setup 2; (c) Setup 3; (d) Setup 4; (e) Setup 5; (f) Setup 6; (g) Setup 7; (h) Setup 8.

In space, the Cartesian coordinate system is used to determine the direction of each measuring point. The X-axis is in the longitudinal direction, the Y-axis is in the bridge’s transverse direction, and the Z-axis is vertical with a positive upward direction. Two sensors with X and Y axes were mounted at each bearing. The sensors were positioned on the Y-axis, Z-axis, or both the Y and Z axes at other points. Specifically, the direction of the measuring points is shown in the Table 1.

The measurement procedure is controlled using a laptop, which also gathers and saves the dynamic responses.

Table 1. DOF at measuring points.

Setup	Reference Point			Moving Point				
Setup 1	103 z	103 y	100 y	100 x	200 y	200 x	101 y	101 z
Setup 2	103 z	103 y	102 y	102 z	104 y	104 z	201 z	202 z
Setup 3	103 z	103 y	105 y	105 z	106 y	106 z	204 z	205 z
Setup 4	103 z	103 y	107 y	107 z	108 y	108 z	205 z	206 z
Setup 5	103 z	103 y	109 y	109 z	110 y	110 z	207 z	208 z
Setup 6	103 z	103 y	111 y	111 x	211 y	211 x	209 z	210 z
Setup 7	103 z	103 y	1001 y	1001 x	1002 y	1003 y	1003 x	1004 y
Setup 8	103 z	103 y	1005 y	1006 y	1007 y	1008 y	1009 y	1010 y

3.2.2. Data Processing and Feature Extraction

The MACEC toolbox [53] was used to analyse all of the measurement data. First, the data needed to be pre-processed. A measuring grid was created on the MACEC system. The measuring points were assigned and numbered, corresponding to the actual measuring points. Input parameters, such as sensor label, sensitivity, data, and distance to each measuring point, were assigned. Such measured signal data are often skewed and do not coincide with the balance axis; the remove-offset function removes these components from the measurement data. The obtained dynamic signal was taken from the time domain and represented in the frequency domain using the Fast Fourier Transform (FFT) algorithm (Figure 6).

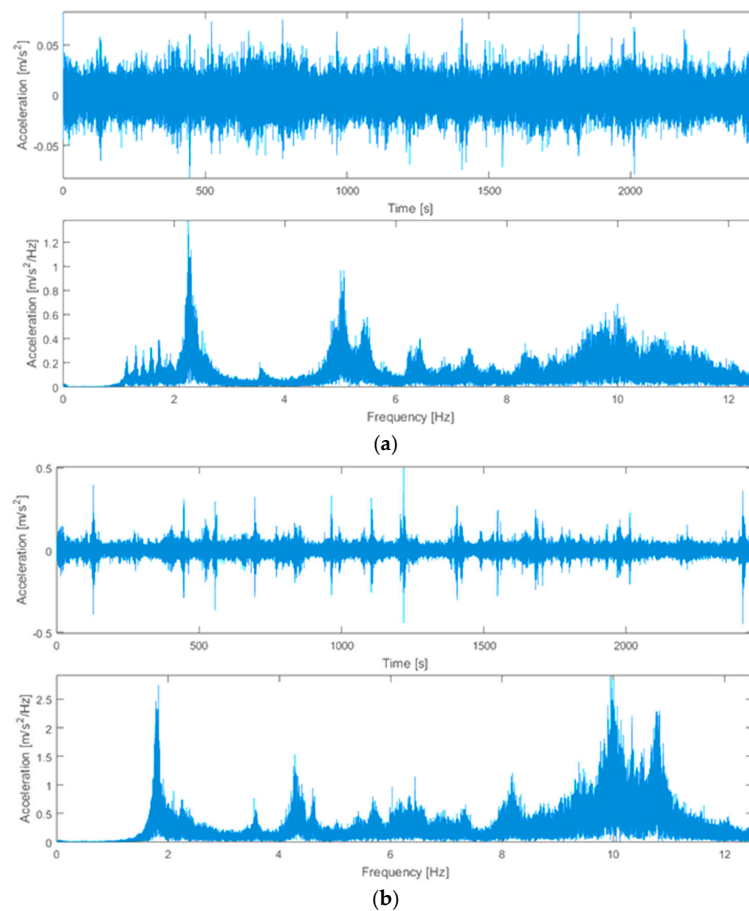


Figure 6. Dynamic response sensor in: (a) time domain and (b) frequency domain.

Based on input data, as well as data obtained from pre-processing (noise removal, and data classification into corresponding nodes), a model with complete data for measurement points was formed. System identification was accomplished using the covariance-based

stochastic subspace identification (SSI-COV) technique. Based on knowledge from numerous similar constructs, the following criteria were selected to concretise and characterise the modality: frequency stabilisation (1%), damping ratio stabilisation (5%), and mode shape stabilisation (1%). The stabilisation diagrams (Figure 7) were then constructed.

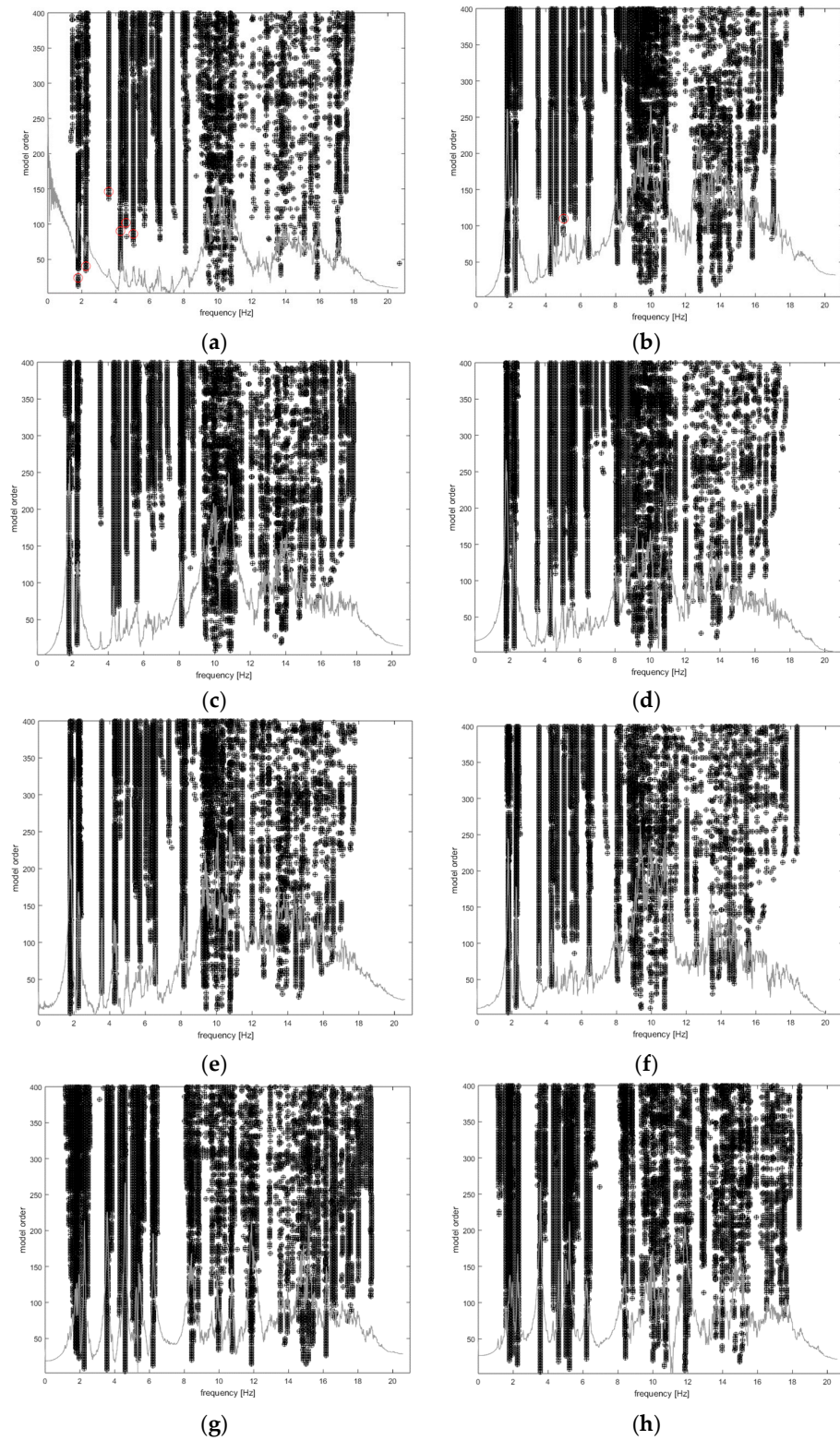


Figure 7. Stabilisation diagrams for the eight setups: (a) Setup 1; (b) Setup 2; (c) Setup 3; (d) Setup 4; (e) Setup 5; (f) Setup 6; (g) Setup 7; (h) Setup 8.

The choice of stable poles (marked by the dashed red lines) was based on their obvious appearance in the eight setups (Figure 8). The corresponding frequency and mode shape could be determined for each selection via MACEC.

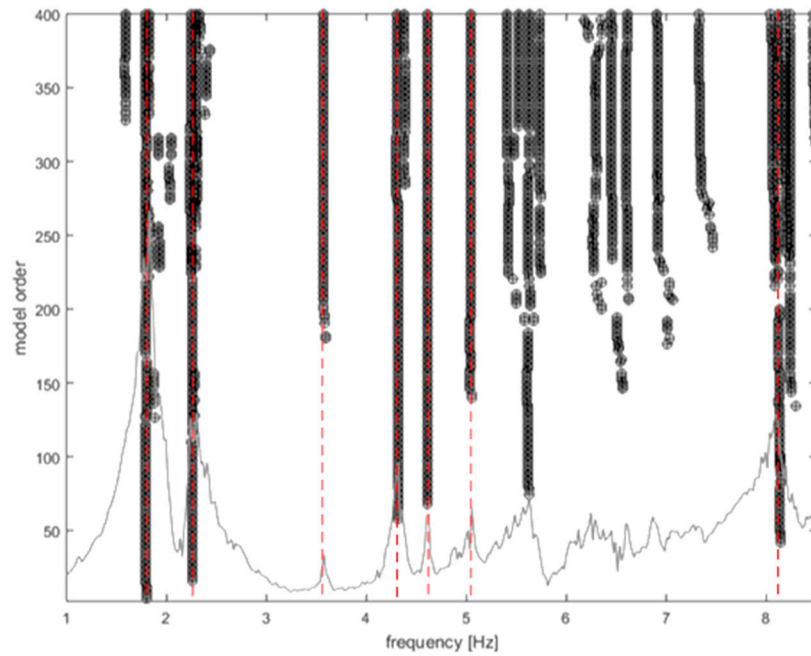


Figure 8. Stabilisation diagram in an interval from 1 to 8.5 Hz.

After data processing, the shape of the seven identified modes were identified from the campaigns. Figure 9 displays mode shapes from eight setups:

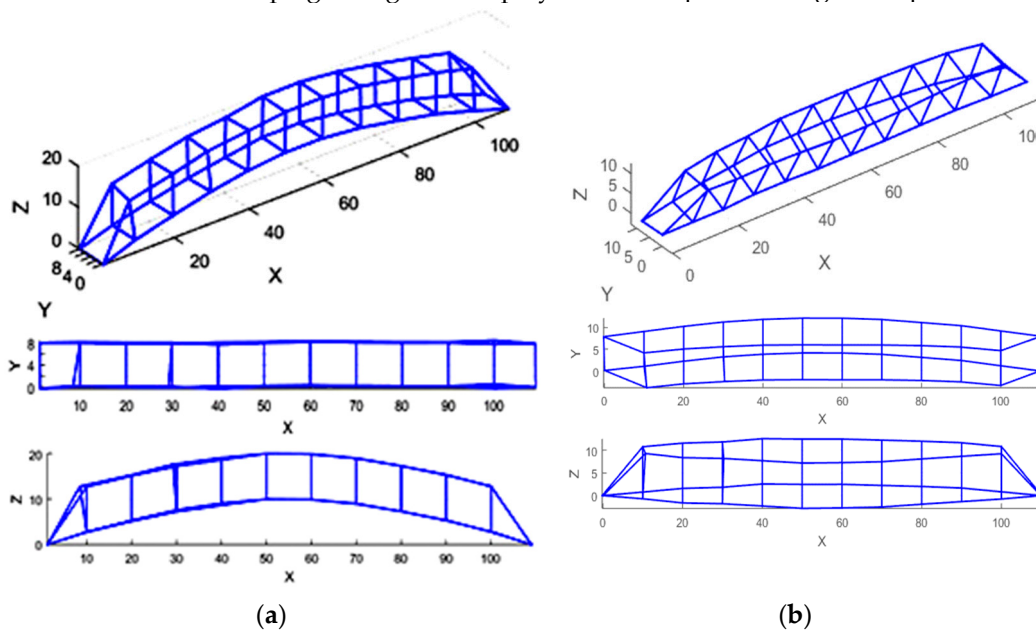


Figure 9. Cont.

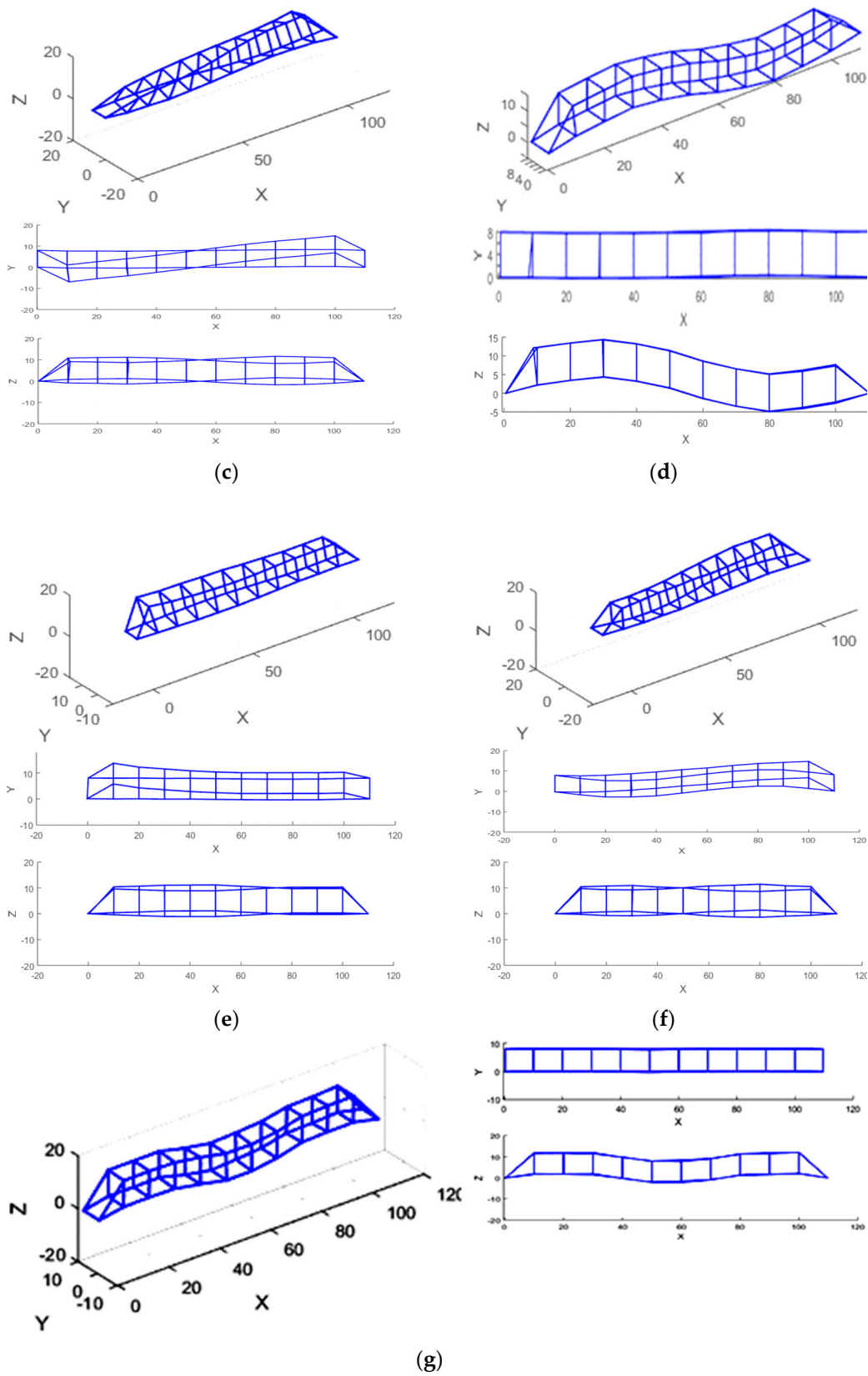


Figure 9. Mode shapes of Chuong Duong bridge in the campaigns: (a) Mode 1: $f = 1.79$ [Hz] (1st vertical bending); (b) Mode 2: $f = 2.25$ [Hz] (1st lateral); (c) Mode 3: $f = 3.57$ [Hz] (2nd torsion); (d) Mode 4: $f = 4.30$ [Hz] (2nd vertical bending); (e) Mode 5: $f = 4.60$ [Hz] (lateral movement); (f) Mode 6: $f = 5.03$ [Hz] (2nd lateral bending); (g) Mode 7: $f = 8.09$ [Hz] (3rd vertical bending).

From these different setups, seven modes could be identified. Their natural frequencies and damping ratios can be found in the Table 2.

Table 2. Frequency values of the seven identified modes.

No.	Frequencies [Hz]	Damping Ratios [%]	Modal Phase Collinearity	Mode Type
1	1.79	1.50	0.999	First vertical bending
2	2.25	1.06	0.998	First lateral
3	3.57	0.77	0.999	Second torsion
4	4.30	1.21	0.999	Second vertical bending
5	4.60	0.40	0.996	lateral movement
6	5.03	1.50	0.998	Second lateral bending
7	8.09	1.06	0.997	Third vertical bending

The standard deviation of the natural frequency was calculated to assess the defined modes' effectiveness. Because these standard deviation of natural frequency values were low, each setting's system recognition quality was high. Modal phase alignment (MPC) measured the mode shape's departure from actual values, with MPC = 1 corresponding to the pure real mode. Every MPC value was higher than 0.998. A structure with light and/or proportional damping physics modes was likely to be realistic, so the elevated MPC result typically indicated a mode that had been precisely defined.

3.3. FEM Creation and Updating

3.3.1. Initial FE Model

A FE model of Chuong Duong bridge was built, taking into account the bridge's structure (Figure 10) [54].

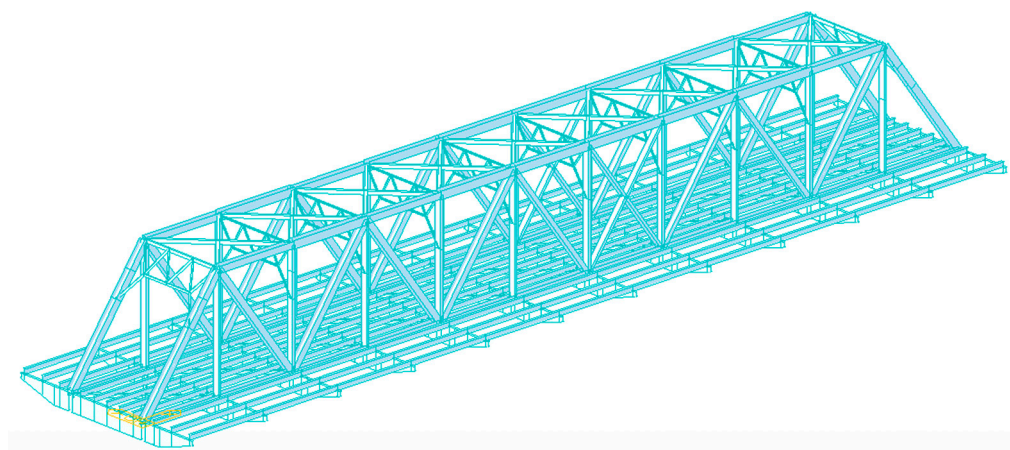


Figure 10. FEM of Span 8 of the Chuong Duong bridge.

Top chords, bottom chords, cantilevers, gate frames, and verticals (all of which were modelled using three-dimensional beam elements), made up the principal structural components. Other components, such as wind bracing, stiffening frame, and longitudinal linkage, were modelled with truss elements. The global X-axis of the bridge was in its longitudinal direction, the Z-axis was vertical, and the Y-axis was the transverse (to the direction of the river flow). The built model consisted of 619 elements, which included 461 beam elements and 158 truss elements. Six degrees of freedom (DOF) were available for each element node, and these DOFs corresponded to translational and rotational displacements in the X, Y, and Z axes. Table 3 shows the types of elements used in the finite element model:

Table 3. List of element types.

No.	Type of Element	Number of Elements	Properties	
			Cross Sections	Material
1	Beam element	461	Top chords, bottom chords, cantilevers, and gate frames	Steel
2	Truss element	158	Wind bracing, stiffening frame, and longitudinal linkage	Steel

The input parameters of the material (Young's modulus, specific gravity) as well as of the section (area, moment of inertia) were referenced from the as-built records. Specifically: Young's modulus of steel (beams, truss rods, cantilever) $E_s = 200$ Mpa; the density of steel $\rho_s = 7850$ kg/m³. Nonstructural elements, such as the bridge deck, balustrades, lighting systems, and plumbing, were included in the model as additional mass. Typical cross-sections of some truss members are shown in Table 4.

Table 4. Cross-section of truss members.

No.	Truss Members	Area (mm ²)	Moment of Inertia I_y (mm ⁴)	Moment of Inertia I_z (mm ⁴)
1	Bridge gate frame	4.27×10^4	2.9×10^9	1.15×10^9
2	Top lateral bracing	4.75×10^4	3.31×10^9	1.75×10^9
3	Bottom lateral bracing	4.75×10^4	3.31×10^9	1.75×10^9
4	Struts	1.83×10^4	1.03×10^9	5.29×10^7
5	Diagonal chords	4.17×10^4	2.82×10^9	1.04×10^9
6	Vertical chords	1.83×10^4	1.03×10^9	5.29×10^7
7	Top chords	1.83×10^4	1.03×10^9	5.29×10^7
8	Bottom chords	1.83×10^4	1.03×10^9	5.29×10^7

Boundary Conditions: The Dirichlet boundary conditions of the numerical model were created to accurately reflect the boundary conditions of the actual structure. The span of eight bridges in Chuong Duong included two types of bearings (Figure 11). Based on the survey results, the displacement constraints of the model were made, corresponding to the actual displacement capacity of the bearing.



(a)

(b)

Figure 11. Two types of bearing were used in the eighth span of the Chuong-Duong Bridge: (a) type 1; (b) type 2.

The first type of bearing (movable bearing) allowed for vertical and horizontal displacement (with some constrain according to the bearing design profile), while restricting longitudinal displacement. The second type of bearing (fixed bearing), which limits vertical and longitudinal displacement, allowed for small horizontal displacements. All supports allowed vertical rotation, and limited other directions.

Utilising the block Lanczos method, the FE model for dynamic analysis was carried out. Figure 12 and Table 5 display some of the mode forms' mode shapes and natural frequencies.

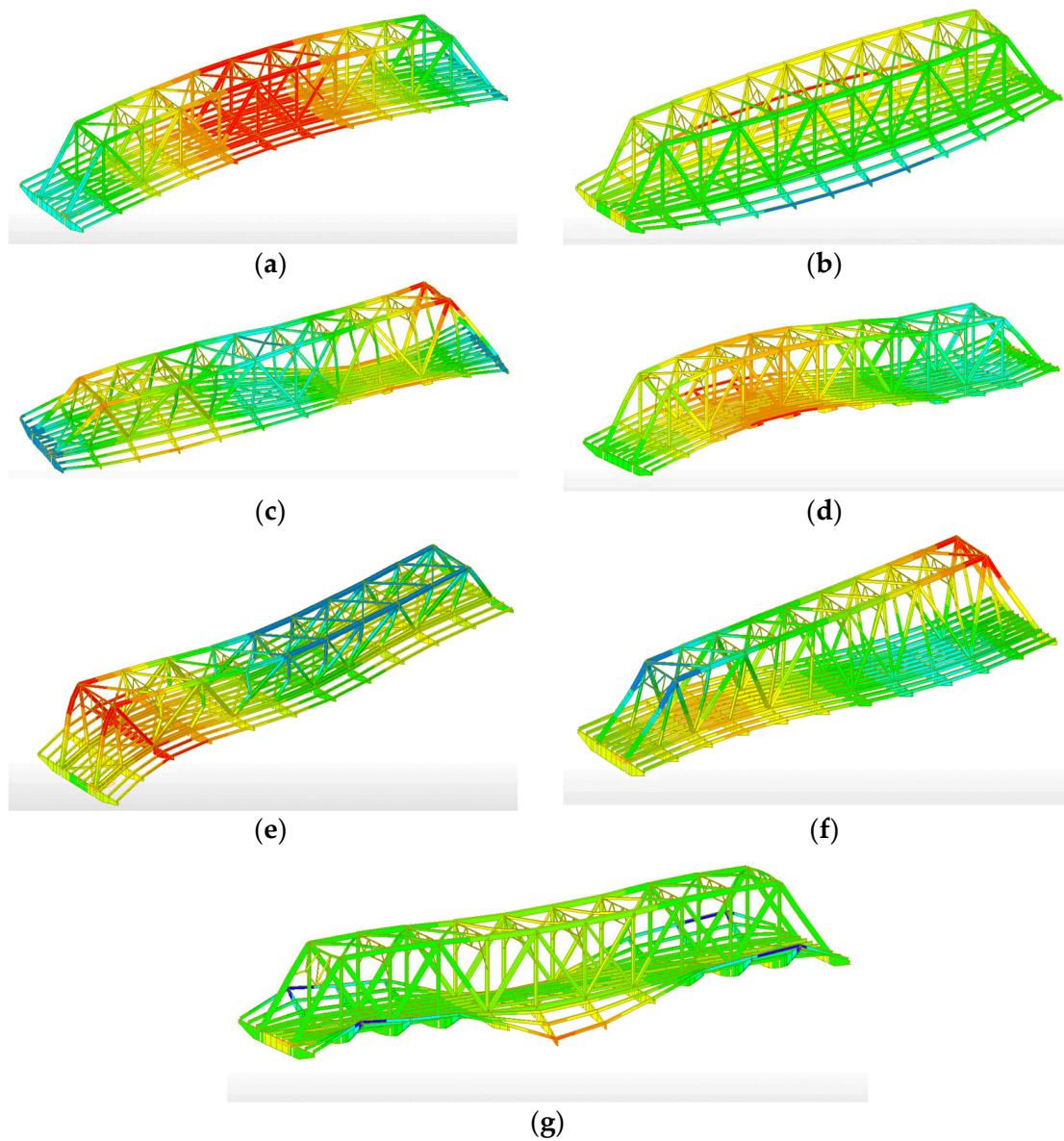


Figure 12. Seven first mode shapes from simulation: (a) Mode 1: $f = 1.83$ [Hz] (1st vertical bending); (b) Mode 2: $f = 2.34$ [Hz] (1st lateral); (c) Mode 3: $f = 3.45$ [Hz] (2nd torsion); (d) Mode 4: $f = 4.06$ [Hz] (2nd vertical bending); (e) Mode 5: $f = 4.52$ [Hz] (lateral movement); (f) Mode 6: $f = 5.16$ [Hz] (2nd lateral bending); (g) Mode 7: $f = 8.39$ [Hz] (3rd vertical bending).

Table 5. Natural frequency and mode shapes of numerical model.

Mode	f-Simulation (Hz)	f-Measurement (Hz)	Error (%)	MAC	Type
1	1.83	1.79	2.23	0.87	1st vertical bending
2	2.34	2.25	4	0.85	1st lateral
3	3.45	3.57	3.36	0.86	2nd torsion
4	4.06	4.30	5.58	0.69	2nd vertical bending
5	4.52	4.60	1.74	0.83	lateral movement
6	5.16	5.03	2.58	0.72	2nd lateral bending
7	8.39	8.09	3.71	0.69	3rd vertical bending

The Modal Assurance Criterion (MAC), a statistical indicator, is particularly sensitive to significant discrepancies in the mode shapes and is comparatively insensitive to smaller differences [55]. This results in a reliable statistical indication and consistency between the mode shapes. This study used the MAC value to evaluate and update the finite element model. The Formula (26) was used to calculate the MAC value:

$$MAC = \frac{\left| \sum_{k=1}^n (\tilde{\varphi}_k)^T \times \varphi_k \right|^2}{\left\{ \sum_{k=1}^n (\tilde{\varphi}_k)^T \times \varphi_k \right\} \times \left\{ \sum_{k=1}^n (\varphi_k)^T \times \varphi_k \right\}} \tag{26}$$

where n is the number of modes shape considered, MAC is the modal assurance criterion, $\varphi_k, \tilde{\varphi}_k$ is the modes shape FEM and experimental, and T represents the transposed matrix.

The MAC values were determined through Formula (26), comparing the FE model results and the actual measurements. The first three MAC values greater than 0.85 showed good agreement between each pair of mode shapes. However, other MAC values did not reach this minimum value. The correlation between the calculated and measured mode shape vectors was not guaranteed. The frequency values were also significantly different. This is a common situation for initial FE models, most of which have not been able to extract modes with high accuracy. Meanwhile, depending on the calculation requirements of the structure, some structures needed high accuracy to structure health monitoring, diagnose damage. There were many uncertain parameters, such as material properties and stiffness parameters. For this reason, we recommend performing a model update procedure to reduce errors.

3.3.2. Update Model Parameters through Particle Swarm Optimisation (PSO) Algorithm

The particle swarm optimization (PSO) algorithm was established and developed on the principles of swarm intelligence, in order to find solutions for optimisation problems in a particular search space [56,57]. To understand the PSO algorithm better, observe a simple example of a flock of birds foraging. The foraging space is now the entire three-dimensional space. At the beginning of the search, the whole flock flies in a certain direction, which can be very random. However, after a period of searching, some individuals in the herd began to find a place containing food. Depending on the amount of food discovered, the individual sends a signal to the other individuals searching in the vicinity. This signal propagates throughout the population. Based on the information received, each individual will adjust both their flight direction and speed in the direction of where there is the most food. Such communication is often viewed as a phenotype of herd intelligence. This mechanism helps the whole flock of birds to find out where there is the most food in extremely large search spaces.

In swarm optimization, each particle searches a space by itself, remembering the best value, and informing other individuals. Other instances will receive the information and decide to continue the search or report its location so that other instances continue to act. Consequently, values in the search space are obtained quickly and accurately. There are two parameters that are particularly important: the location of an instance, and the search velocity. These two parameters are expressed through the formulas for updating the position and updating the velocity of the instance:

$$x^i(t + 1) = x^i(t) + v^i(t + 1) \tag{27}$$

$$v^i(t + 1) = wv^i + C_1r_1(p^i(t) - x^i(t)) + C_2r_2(G_{best} - x^i(t)) \tag{28}$$

where x^i is the position of instance i at different times (t and $t + 1$); v^i is the speed of individual i ; w is the parameter of inertial weight; C_1 and C_2 represent the population's cognitive coefficient; r_1 and r_2 are random numbers in the range $[0, 1]$; $p^i(t)$ is the best position

of each individual; G_{best} is the best location of the entire population. Each individual is characterised using its velocity vector and its position in space.

To evaluate the similarity between the FE model and the practical structure, an objective function was built based on the natural frequency and the mode shape of the structure:

$$Fitness = \sum_{k=1}^n [1 - MAC(\varphi_k, \tilde{\varphi}_k)] + \sum_{k=1}^n \frac{\omega_k^2}{\tilde{\omega}_k^2} = \sum_{k=1}^n \left[1 - \frac{(\tilde{\varphi}_k^T \varphi_k)^2}{(\varphi_k^T \varphi_k)(\tilde{\varphi}_k^T \tilde{\varphi}_k)} \right] + \sum_{k=1}^n \frac{(\omega_k - \tilde{\omega}_k)^2}{\tilde{\omega}_k^2} \tag{29}$$

In the case of Chuong Duong bridge, determining material parameters required many experiments. At the same time, the masses of nonstructural parts were also difficult to determine accurately. Some uncertain parameters have been selected to update the numerical model. Based on experience, Table 6 shows the range of variation for the uncertain parameters.

Table 6. Uncertain parameters.

No.	Uncertain Parameters	Initial Value	Upper Bound	Lower Bound
1	Young’s modulus —Steel E_s (GPa)	200	210	190
2	Weight density —Steel ρ_s (kg/m ³)	7850	8000	7800
3	Masses of non-structural — m_b (kg/m)	3000	3000	5000

The updated uncertainty parameters and FE model after using the PSO are presented in Table 7.

Table 7. Updated parameters.

No.	Uncertain Parameters	Initial Value	Updated Value
1	Young’s modulus —Steel E_s (GPa)	200	205.54
2	Weight density —Steel ρ_s (kg/m ³)	7850	7956.5
3	Masses of non-structural — m_b (kg/m)	3000	3600

The results after updating show that updating the model lowered the discrepancy between the calculated and measured natural frequencies, and the MAC value reached a good level (Table 8).

Table 8. Summary of natural frequency and mode shapes of the plate structure, after being updated.

Mode	f-Simulation (Hz)	f-Measurement (Hz)	Error (%)	MAC	Type
1	1.79	1.79	0.00 ↓	0.99 ↑	1st vertical bending
2	2.24	2.25	0.44 ↓	0.95 ↑	1st lateral
3	3.58	3.57	0.28 ↓	0.96 ↑	2nd torsion
4	4.33	4.30	0.69 ↓	0.94 ↑	2nd vertical bending
5	4.61	4.60	0.21 ↓	0.94 ↑	lateral movement
6	5.05	5.03	0.39 ↓	0.94 ↑	2nd lateral bending
7	8.15	8.09	0.74 ↓	0.94 ↑	3rd vertical bending

The MAC values of the FE model before and after the update are shown in Figure 13. After being updated, the accuracy of the model increased a lot. These MAC values show good agreement between the FE and the actual models.

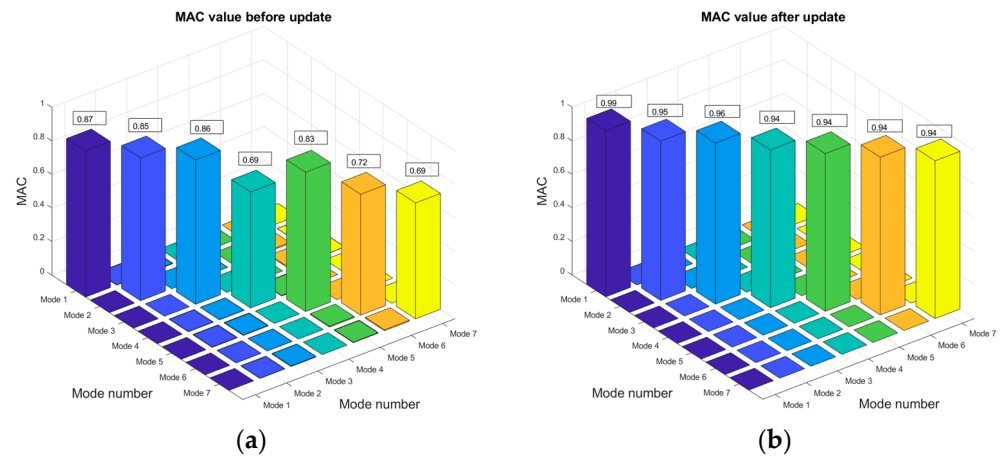


Figure 13. MAC values: (a) before the model was updated; (b) after updating.

Figure 14 shows that before updating the model, the calculation results and natural frequency measurement results had high errors. After updating the model, the error of the natural frequency between calculation and measurement decreased significantly, and the model became highly accurate and reliable.

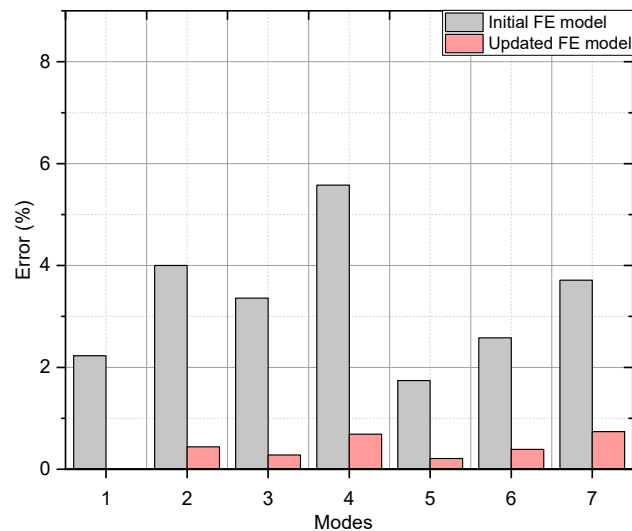


Figure 14. Frequency differences before and after updating.

The calculation results show that, after about 30 iterations performed using PSO, the model parameters began to converge and give good results, minimising the process of testing parameters in the modelling. After being updated, the numerical model was accurate, being almost the same as the actual object. This model was employed for creating data to train the ANN.

3.4. Generate Data and Train the ANN Model

3.4.1. Single Damages

Three layers made up the ANN’s architecture in this study: an input layer, a hidden layer, and an output layer. The first seven modes’ frequencies were used as input data for various damage situations, and the output data comprised damage locations and levels (Figure 15).

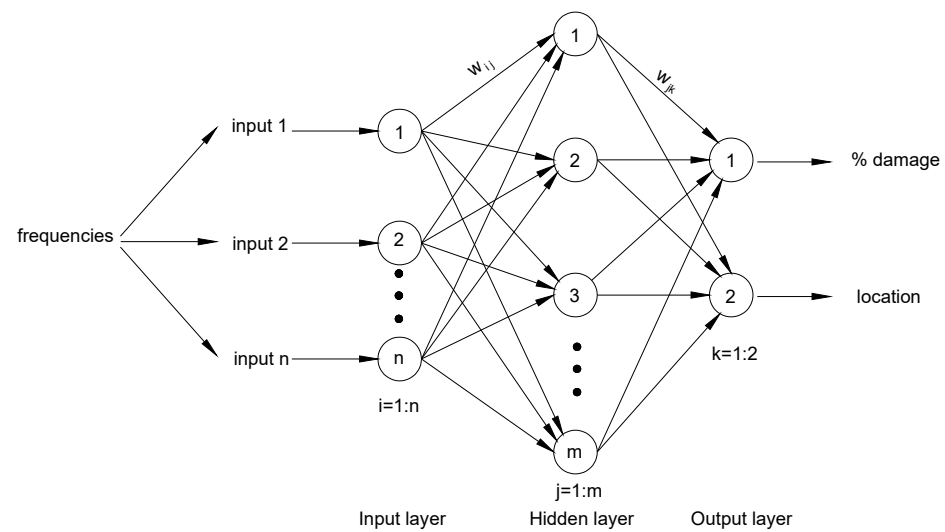


Figure 15. Architecture of the ANN used in this study.

The updated model's modal analysis created input and output data for the ANN. The elements' stiffness was decreased in order to create scenarios of structural damage. With a 1% interval, the elements' stiffness decreased from 0% to 50%. Damage is only truly dangerous and sensitive enough when it occurs on major structural components. Therefore, only the main truss rods were considered in this case. The following equation determined the quantity of input data needed to train the network:

$$N = n_e \times n_s \quad (30)$$

where n_e = total of elements that were considered, and n_s = the number of damage scenarios occurring for a single element. If 84 main elements of the truss are considered, the input data will consist of 4200 samples.

The ANN was then configured to the settings for training the network after the data generation. The results of the network training process were significantly influenced by the number of neurons in the hidden layer. If the ANN had too few hidden layers, the ANN was too simple and would struggle to deal with the problems to be solved. In contrast, if ANN had too many hidden layers, the network was too complicated. Computer resources consume a lot, which easily leads to overfitting. The loop was used to choose the ideal number of hidden layers within the range of 1 to 50, i.e., the number of hidden layers that will be selected by the loop. Additionally, the impact of noise was evaluated in all situations with a level of 2% for natural frequencies. The Levenberg–Marquardt backpropagation algorithm was used by the ANN to train the network. For damage identification, a data split in the training procedure of 70%–15%–15% was used. There were a maximum of 1000 epochs. In the case of epochs greater than 1000 but still not reaching the best value, it was necessary to implement network optimisation solutions.

After training, the following figures demonstrate how the ANN model performed:

All training cases with regression values more than 0.99 are displayed in Figure 16. The training, evaluation, and test datasets are located along the target line (45-degree line). This demonstrates that the real value and predicted value were almost similar. The regression values (R) in linear regression models always range from 0 to 1. The estimated and desired outcomes were the same if R was near to the upper bound (1). Figure 17 shows the histogram of the calculated and intended output errors. There was very little variance between the target and the output. Figure 18 shows the training performance in the datasets. The best validation performance value of 3.0179 was achieved at epoch 190. The epoch number did not exceed 1000, and such network optimisation was not necessary. The graph also shows that the values in the data sets were quite convergent, and no overfitting phenomenon occurred. From the performance graph of R-values, MSE

(Tolerance), and the error histogram, the model had clearly been successfully trained, and can thus be applied to the real bridge.

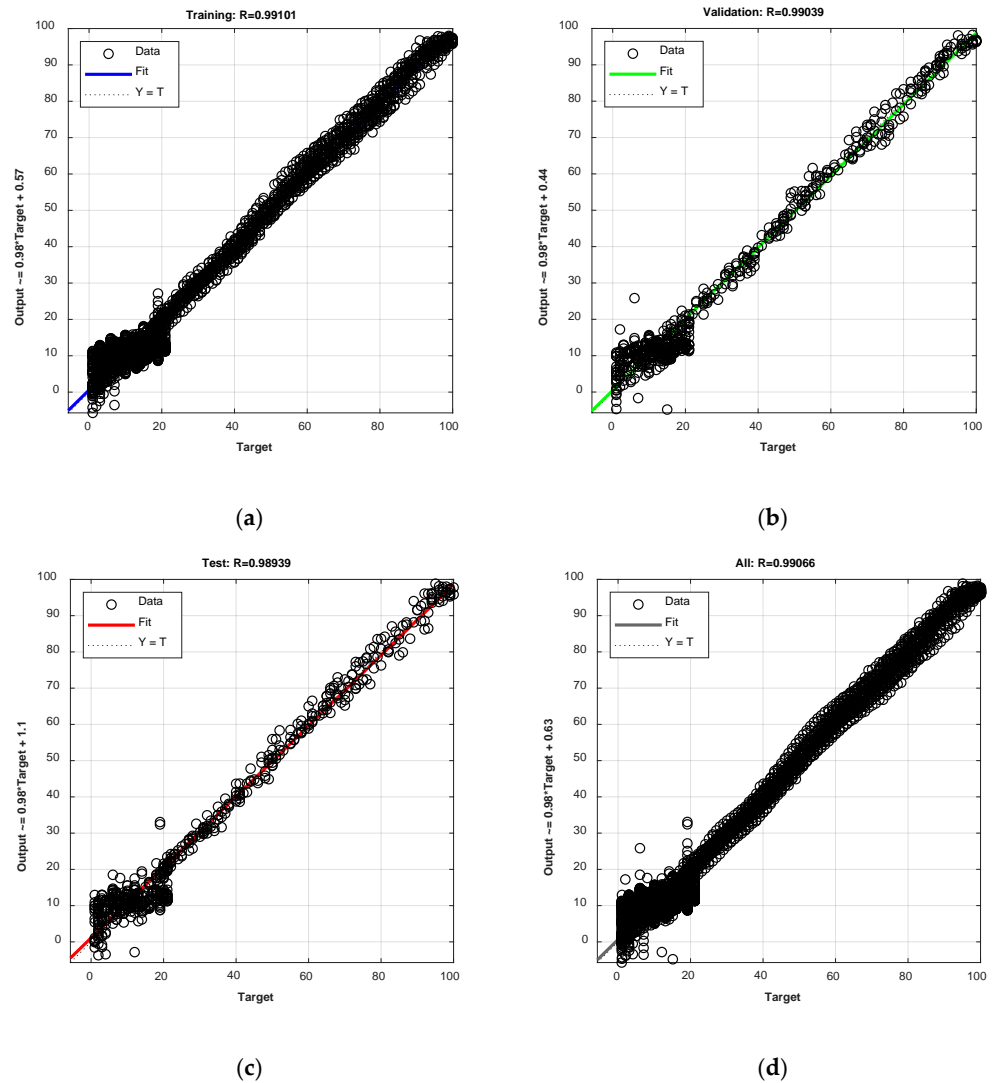


Figure 16. Regression values of ANN in single damage case: (a) Training; (b) Validation; (c) Test; (d) All data.

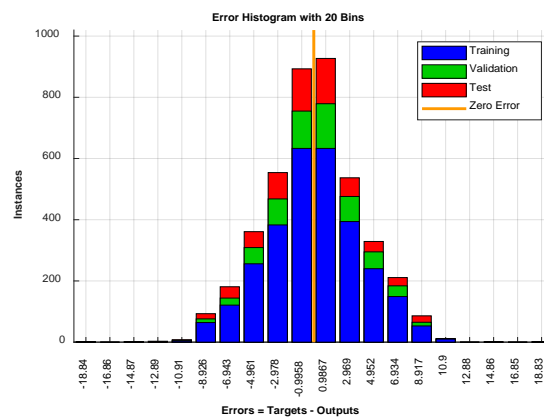


Figure 17. Error histogram of ANN in single damage case.

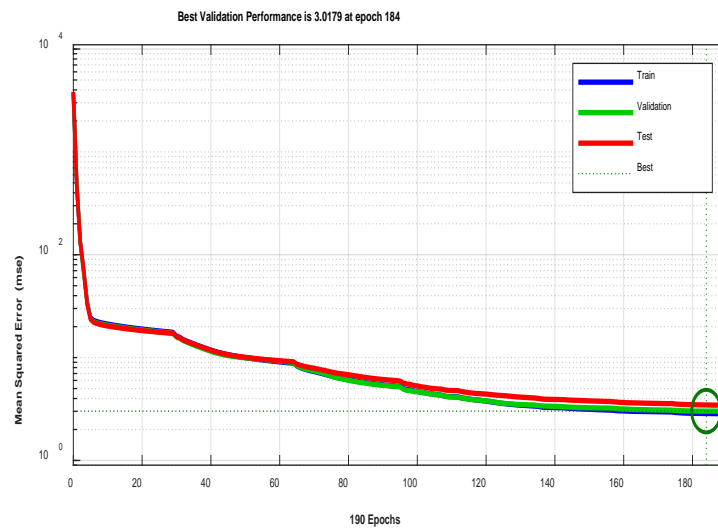


Figure 18. Tolerance of network in a case of single damage.

3.4.2. Two Damaged Elements

Damages were simultaneously generated in two random elements. For each element, a damage level was assigned from 0% to 50% with a 1% interval. In this study, the failures at the elements were assumed to be the same. The amount of data was calculated according to the formula:

$$N = n_s \times \frac{n_e!}{2! \times (n_e - 2)!} \tag{31}$$

The total amount of data generated comprised 174,300 samples.

Figure 19 shows that the *R*-value of the network using ANN was 0.986. The training, validation, and test datasets follow the regression line.

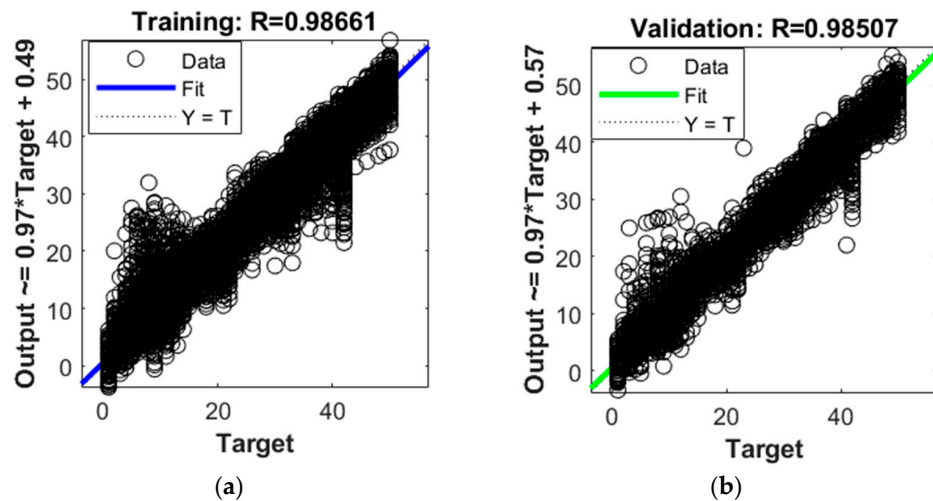


Figure 19. Cont.

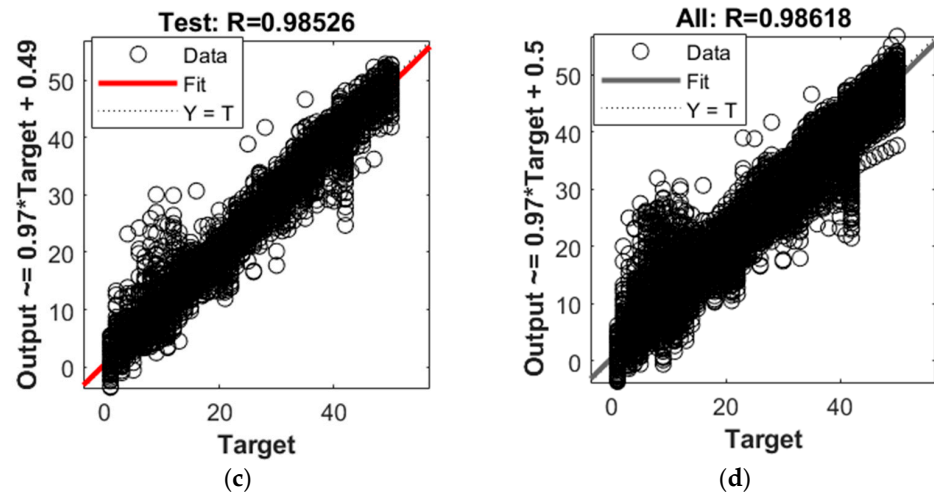


Figure 19. Regression values of ANN in cases with two damaged elements: (a) Training; (b) Validation; (c) Test; (d) All data.

According to Figures 20 and 21, there were small deviations from the zero-error line between computed and desired values. The results we obtained showed a good agreement between predicted and actual outputs.

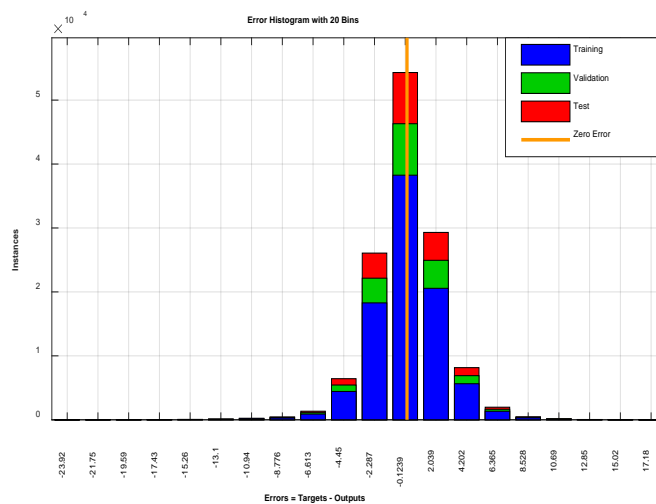


Figure 20. Error histogram of ANN in cases with two damaged elements.

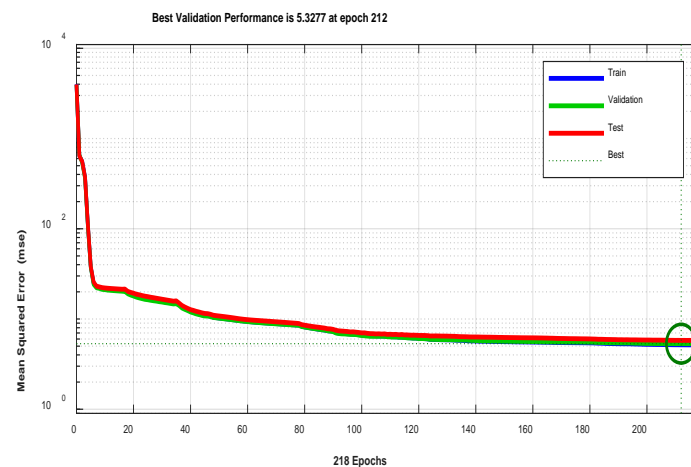


Figure 21. Tolerance of network of ANN in two cases of damaged elements.

3.5. The Service of the Trained ANN Model in Actual

3.5.1. Single Damage

Normally, to detect and locate the damage of the bridge structure, a comprehensive survey investigation would be carried out. After the survey, experts make a computational model and evaluate. Such work requires a lot of human resources and costs a lot of money. Even when considering only the measurement of the vibration of the entire span structure, the implementation of the setups measurements as described above also requires a lot of work. Instead, using an artificial neural network offers a huge advantage.

The use of a trained network can be applied to the actual span structure of Chuong Duong bridge. During servicing, there was an accident on Chuong Duong bridge that affected the bridge structure (Figure 22).

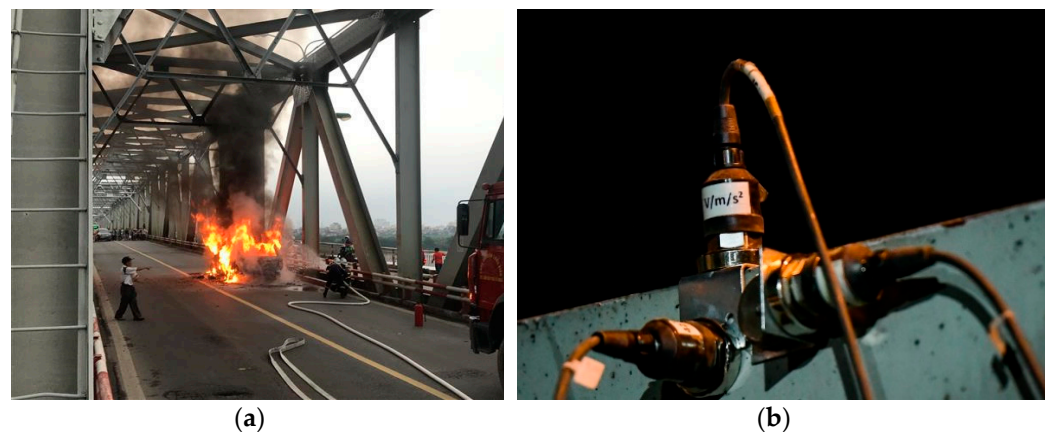


Figure 22. (a) Collision and damage at a truss rod; (b) Experiment to determine the natural frequency of the bridge.

A simple experiment was conducted, since only the structure's natural frequency needs to be ascertained. A single vibration measurement point in three directions was located on Chuong Duong bridge (Figure 22). With only one measuring point, the natural frequency of Chuong Duong bridge was identified. Although it was not possible to identify the mode shapes of the bridge, with the trained ANN it was possible to locate and quantify the damage.

The results of the natural frequencies of the first seven mode shapes determined through the experiment were [1.229; 2.4167; 4.1954; 4.2623; 4.5925; 6.2147; 7.7865]. These results were used as the input for feeding the trained network. Results after putting data into the network returned [25; 6]. This meant that 25% damage was detected at element 6 (truss number 6). It is easy to see that the result of locating damage at element 6 was correct. According to the report of the UCT company (who performed the calculation of damage assessment), the damage level of truss rod was 30%. Results using the ANN were relatively accurate. This is a case of damage that was easy to identify and recognise in practice. However, for cases where the damage location is difficult to detect (for example, if the damage is located in prohibitively high or difficult to reach locations, such as the middle of the river), the ANN will show its advantages.

3.5.2. 2 Damaged Elements

In this study, a hypothetical failure was generated on the updated finite element model. Two elements (10 and 15) were assumed to be 40% damaged. Putting the data into the trained ANN model, the network detected and returned the result 39% at element 10 and 15. Although not 100% accurate, the trained network detected the location and was relatively close to the simulation results.

4. Conclusions

This study investigated artificial intelligence-based structural health monitoring. Through testing and practical application in a steel truss bridge, it achieved potential performance, in terms of structural monitoring. Along with the detailed explanation in this paper, some main conclusions can be derived:

- By combining the vibration measurement results of the structure with the artificial neural network, routine structural health monitoring tasks could be reduced. Specifically, an artificial neural network trained using the vibration measurement results were able to localise and quantify preliminary damage, minimising logistics. In this study, the test was applied to a large steel truss bridge in Vietnam (Chuong Duong Bridge). The results show the potential of the method in similar bridges.
- The results of the comprehensive vibration measurement of the structure were used for the first time to update the structure; as such, this took time and effort, but this requirement could be reduced many times over in future checks.
- An initial FE model was created and updated based on the modal characteristics extracted from the field vibration measurement experiment. Using the PSO algorithm, an FE model with a behaviour close to reality was built. Before the update, the FE model had a big difference from the actual measurement (the biggest difference in frequency was 5.58%, the MAC value was only 0.87). After updating, the similarity between the FE model and the experiment increased significantly (the biggest difference in frequency being 0.74%, MAC value increasing to the lowest value of 0.94).
- Based on the updated model, damage scenarios were performed, and data was extracted for input into the ANN. In this study, damages were performed on the model by reducing the stiffness of the main elements.
- Creating and organising data from a finite element model is very important if one wants to get good results when training ANNs. With a large number of samples, training the network takes time, but the improved effects after training can make up for this.
- Compared with other methods, this approach had various advantages: saving human resources; being able to identify damage in hard-to-detect locations; and reducing the number of measuring points in the case of vibration tests.
- In the case study of this research, with a single damage, the ANN was able to identify and quantify the damage relatively accurately. For damage occurring on two elements, since there is no actual data, the network usage after training was measured on the model. The results were quite satisfactory. The case using the data of two simultaneous damages seemed to be more accurately predicted using the network. This can be explained because actual experimental data will more or less have noise, in addition to being simultaneously affected by many factors. Meanwhile, the data used to confirm the case of two damages at the same time was taken directly from the model.
- In future studies, the authors will implement a number of different types of structures, such as cable-stayed bridges, suspension bridges, and continuous bridges. At the same time, the current training of artificial neural networks is also quite time consuming, with large data sets. Further studies will also focus on solving this problem by applying algorithms combined with ANN.

Author Contributions: Conceptualisation, M.Q.T., J.M., H.X.N., T.V.N. and H.S.S.; methodology, M.Q.T., J.M., T.V.N. and H.X.N.; software, M.Q.T., B.D.N. and S.N.D.; validation, J.M. and S.N.D.; formal analysis, Q.T.N.; investigation, E.B., M.Q.T. and S.N.D.; resources, E.B.; data curation, S.N.D.; writing—original draft preparation, M.Q.T. and S.N.D.; writing—review and editing, M.Q.T., J.M. and S.N.D.; visualisation, B.D.N. and M.Q.T.; supervision, J.M., H.S.S., H.X.N. and T.V.N.; project administration, J.M. and S.N.D.; funding acquisition, J.M., E.B. and S.N.D. All authors have read and agreed to the published version of the manuscript.

Funding: This research was funded by FCT/MCTES through national funds (PIDDAC) from the R&D Unit Institute for Sustainability and Innovation in Structural Engineering (ISISE), under the reference UIDB/04029/2020, and from the Associate Laboratory Advanced Production and Intelligent Systems ARISE, under the reference LA/P/0112/2020, as well as financial support of the project research “B2022-GHA-03” from the Ministry of Education and Training. And The APC was funded by ANI (“Agência Nacional de Inovação”) through the financial support given to the R&D Project “GOA Bridge Management System—Bridge Intelligence”, with reference POCI-01-0247-FEDER-069642, which was cofinanced by the European Regional Development Fund (FEDER) through the Operational Competitiveness and Internationalisation Program (POCI).

Data Availability Statement: Not applicable.

Acknowledgments: Minh Q. Tran acknowledges the support by the doctoral grant reference PRT/BD/154268/2022, financed by Portuguese Foundation for Science and Technology (FCT), under the MIT Portugal Program (2022 MPP2030-FCT). Helder S. Sousa acknowledges the funding of FCT through the Scientific Employment Stimulus—4th Edition. The work of Huan X. Nguyen was supported by the VinGroup Innovation Fund (VinIF) under Grant VINIF.2021.DA00192.

Conflicts of Interest: The authors declare no conflict of interest.

References

1. Encardio Rite Group [Updated] A Guide on Geodetic Survey and Monitoring—Encardio Rite. Available online: <https://www.encardio.com/blog/a-guide-on-geodetic-survey-and-monitoring> (accessed on 30 May 2023).
2. Beshr, A.A.E.-W. Structural Deformation Monitoring and Analysis of Highway Bridge Using Accurate Geodetic Techniques. *Engineering* **2015**, *7*, 488–498. [CrossRef]
3. Eteje, S.O. Detailed Geodetic Technique Procedures for Structural Deformation Monitoring and Analysis. *Int. J. Sci. Technol. Res.* **2020**, *6*, 7–23. [CrossRef]
4. Liu, S.; Liu, X.; Yang, F. Control Surveying and Structural Health Monitoring Applied in Large Bridge. *Adv. Mater. Res.* **2013**, *639–640*, 243–246. [CrossRef]
5. Lienhart, W. Geotechnical Monitoring Using Total Stations and Laser Scanners: Critical Aspects and Solutions. *J. Civ. Struct. Health Monit.* **2017**, *7*, 315–324. [CrossRef]
6. Segalini, A.; Carri, A.; Savi, R. Role of Geotechnical Monitoring: State of the Art and New Perspectives. In Proceedings of the GEO-EXPO, Drustvo za geotehniku u Bosni i Hercegovini, Sarajevo, Bosnia and Herzegovina, 10 October 2017; pp. 19–26.
7. Viola, E.; Bocchini, P. Non-Destructive Parametric System Identification and Damage Detection in Truss Structures by Static Tests. *Struct. Infrastruct. Eng.* **2013**, *9*, 384–402. [CrossRef]
8. Ugalde, U.; Anduaga, J.; Martinez, F.; Iturrospe, A. A SHM Method for Detecting Damage with Incomplete Observations Based on VARX Modelling and Granger Causality. *arXiv* **2016**, arXiv:1602.00557.
9. Martínez, D.; Obrien, E.J.; Sevillano, E. *Damage Detection by Drive-by Monitoring Using the Vertical Displacements of a Bridge. Insights and Innovations in Structural Engineering, Mechanics and Computation, Proceedings of the 6th International Conference on Structural Engineering, Mechanics and Computation, SEMC, Cape Town, South Africa, 5–7 September 2016*; CRC Press: London, UK, 2016; pp. 1915–1918. [CrossRef]
10. Hjeltnad, K.D.; Shin, S. Damage Detection and Assessment of Structures from Static Response. *J. Eng. Mech.* **1997**, *123*, 568–576. [CrossRef]
11. Bakhtiari-Nejad, F.; Rahai, A.; Esfandiari, A. A Structural Damage Detection Method Using Static Noisy Data. *Eng. Struct.* **2005**, *27*, 1784–1793. [CrossRef]
12. Bonopera, M.; Chang, K.-C.; Chen, C.-C.; Lin, T.-K.; Tullini, N. Bending Tests for the Structural Safety Assessment of Space Truss Members. *Int. J. Space Struct.* **2018**, *33*, 138–149. [CrossRef]
13. Doebling, S.W.; Farrar, C.R.; Prime, M.B. A Summary Review of Vibration-Based Damage Identification Methods. *Shock Vib. Dig.* **1998**, *30*, 91–105. [CrossRef]
14. Salawu, O.S. Detection of Structural Damage through Changes in Frequency: A Review. *Eng. Struct.* **1997**, *19*, 718–723. [CrossRef]
15. Khatir, S.; Khatir, T.; Boutchicha, D.; Le Thanh, C.; Tran-Ngoc, H.; Bui, T.Q.; Capozucca, R.; Abdel-Wahab, M. An Efficient Hybrid TLBO-PSO-ANN for Fast Damage Identification in Steel Beam Structures Using IGA. *Smart Struct. Syst.* **2020**, *25*, 605–617.
16. Farrar, C.R.; Doebling, S.W. Damage Detection and Evaluation II. In *Modal Analysis and Testing*; 1999 NATO Science Series, Springer Link; Springer: Berlin/Heidelberg, Germany, 1999; pp. 345–378. [CrossRef]
17. Carden, E.P.; Fanning, P. Vibration Based Condition Monitoring: A Review. *Struct. Health Monit.* **2004**, *3*, 355–377. [CrossRef]
18. Catbas, F.N.; Brown, D.L.; Aktan, A.E. Use of Modal Flexibility for Damage Detection and Condition Assessment: Case Studies and Demonstrations on Large Structures. *J. Struct. Eng.* **2006**, *132*, 1699–1712. [CrossRef]
19. Alvandi, A.; Cremon, C. Assessment of Vibration-Based Damage Identification Techniques. *J. Sound Vib.* **2006**, *292*, 179–202. [CrossRef]

20. Nhung, N.T.C.; Minh, T.Q.; Matos, J.C.; Sousa, H.S. Research and Application of Indirect Monitoring Methods for Transport Infrastructures to Monitor and Evaluate Structural Health. In Proceedings of the 2nd International Conference on Structural Damage Modelling and Assessment, Ghent, Belgium, 4–5 August 2021.
21. Mazurek, D.F. Modal Sensitivity to Damage in Multigirder Bridges. *SPIE* **1997**, *3089*, 1892.
22. Doebling, S.; Farrar, C. Statistical Damage Identification Techniques Applied to the I-40 Bridge over the Rio Grande River. In Proceedings of the International Modal Analysis Conference, Santa Barbara, CA, USA, 2–5 February 1998.
23. Alvandi, A. Contribution à L'utilisation Pratique de L'évaluation Dynamique Pour La Détection D'endommagements Dans Les Ponts. Ph.D. Thesis, 2003, Sciences de l'ingénieur [physics]. Ecole des Ponts ParisTech, Français.
24. Minh, T.Q.; Nhung, N.T.C.; Quyet, N.H.; Helder, S.; Sou, S.; Jose, C. Matos Opportunities and Challenges of Digital Twins in Structural Health Monitoring. In Proceedings of the 4th International Conference on Sustainability in Civil Engineering, Hanoi, Vietnam, 25–27 November 2023.
25. Yang, Y.B.; Yang, J.P. State-of-the-Art Review on Modal Identification and Damage Detection of Bridges by Moving Test Vehicles. *Int. J. Struct. Stab. Dyn.* **2018**, *18*, 1850025. [[CrossRef](#)]
26. Karbhari, V.M.; Lee, L.S. W Vibration-Based Damage Detection Techniques for Structural Health Monitoring of Civil Infrastructure Systems. *Struct. Health Monit. Civ. Infrastruct. Syst.* **2009**, 177–212. [[CrossRef](#)]
27. Farrar, C.R.; Doebling, S.W.; Nix, D.A. Vibrationbased Structural Damage Identification. *Philos. Trans. R. Soc. London. Ser. A Math. Phys. Eng. Sci.* **2001**, *359*, 131–149. [[CrossRef](#)]
28. Minh, T.Q.; Helder, S.S.; Jose, C.M. Application of AI Tools in Creating Datasets from A Real Data Component for Structural Health Monitoring. In *Data Driven Methods for Civil Structural Health Monitoring and Resilience: Latest Developments and Applications*, 1st ed.; CRC Press: Boca Raton, FL, USA, 2023.
29. Khiem, N.T.; Lien, T.V. A Simplified Method for Natural Frequency Analysis of a Multiple Cracked Beam. *J. Sound Vib.* **2001**, *245*, 737–751. [[CrossRef](#)]
30. Nguyen, T.; Chan, T.H.T.; Thambiratnam, D.P. Field Validation of Controlled Monte Carlo Data Generation for Statistical Damage Identification Employing Mahalanobis Squared Distance. *Struct. Health Monit.* **2014**, *13*, 473–488. [[CrossRef](#)]
31. Zhang, Z.; Shankar, K.; Morozov, E.V.; Tahtali, M. Vibration-Based Delamination Detection in Composite Beams through Frequency Changes. *J. Vib. Control* **2014**, *22*, 496–512. [[CrossRef](#)]
32. Jeong, M.-J.; Choi, J.-H.; Koh, B.-H. Isomap-Based Damage Classification of Cantilevered Beam Using Modal Frequency Changes. *Struct. Control Health Monit.* **2014**, *21*, 590–602. [[CrossRef](#)]
33. Gillich, G.R.; Ntakpe, J.L.; Abdel Wahab, M.; Praisach, Z.I.; Mimis, M.C. Damage Detection in Multi-Span Beams Based on the Analysis of Frequency Changes. *J. Phys. Conf. Ser.* **2017**, *842*, 012033. [[CrossRef](#)]
34. Wang, L.; Lie, S.T.; Zhang, Y. Damage Detection Using Frequency Shift Path. *Mech. Syst. Signal Process.* **2016**, *66–67*, 298–313. [[CrossRef](#)]
35. Sha, G.; Radzieński, M.; Cao, M.; Ostachowicz, W. A Novel Method for Single and Multiple Damage Detection in Beams Using Relative Natural Frequency Changes. *Mech. Syst. Signal Process.* **2019**, *132*, 335–352. [[CrossRef](#)]
36. Khan, M.W.; Din, N.A.; Ul Haq, R. Damage Detection in a Fixed-Fixed Beam Using Natural Frequency Changes. *Vibroengineering Procedia* **2020**, *30*, 38–43. [[CrossRef](#)]
37. He, K.; Zhu, W.D. Structural Damage Detection Using Changes in Natural Frequencies: Theory and Applications. *J. Phys. Conf. Ser.* **2011**, *305*, 012054. [[CrossRef](#)]
38. Mohan, V.; Parivallal, S.; Kesavan, K.; Arunsundaram, B.; Ahmed, A.K.F.; Ravisankar, K. Studies on Damage Detection Using Frequency Change Correlation Approach for Health Assessment. *Procedia Eng.* **2014**, *86*, 503–510. [[CrossRef](#)]
39. Worden, K.; Manson, G. The Application of Machine Learning to Structural Health Monitoring. *Philos. Trans. R. Soc. A Math. Phys. Eng. Sci.* **2007**, *365*, 515–537. [[CrossRef](#)]
40. Hakim, S.J.S.; Abdul Razak, H. Adaptive Neuro Fuzzy Inference System (ANFIS) and Artificial Neural Networks (ANNs) for Structural Damage Identification. *Struct. Eng. Mech.* **2013**, *45*, 779–802. [[CrossRef](#)]
41. Nguyen, D.H.; Bui, T.T.; De Roeck, G.; Abdel Wahab, M. Damage Detection in Ca-Non Bridge Using Transmissibility and Artificial Neural Networks. *Struct. Eng. Mech.* **2019**, *71*, 175–183.
42. Kaveh, A.; Maniat, M.; Kaveh, A.; Maniat, M. Damage Detection Based on MCSS and PSO Using Modal Data. *Smart Struct. Syst.* **2015**, *15*, 1253. [[CrossRef](#)]
43. Mares, C.; Surace, C. An Application of Genetic Algorithms to Identify Damage in Elastic Structures. *J. Sound Vib.* **1996**, *195*, 195–215. [[CrossRef](#)]
44. Seyedpoor, S.M. A Two Stage Method for Structural Damage Detection Using a Modal Strain Energy Based Index and Particle Swarm Optimization. *Int. J. Non Linear Mech.* **2012**, *47*, 1–8. [[CrossRef](#)]
45. Yu, L.; Xu, P. Structural Health Monitoring Based on Continuous ACO Method. *Microelectron. Reliab.* **2011**, *51*, 270–278. [[CrossRef](#)]
46. Guo, H.Y.; Li, Z.L. A Two-Stage Method to Identify Structural Damage Sites and Extents by Using Evidence Theory and Micro-Search Genetic Algorithm. *Mech. Syst. Signal Process.* **2009**, *23*, 769–782. [[CrossRef](#)]
47. Hao, H.; Xia, Y. Vibration-Based Damage Detection of Structures by Genetic Algorithm. *J. Comput. Civil Eng.* **2002**, *16*, 222–229. [[CrossRef](#)]
48. Na, C.; Kim, S.P.; Kwak, H.G. Structural Damage Evaluation Using Genetic Algorithm. *J. Sound Vib.* **2011**, *330*, 2772–2783. [[CrossRef](#)]

49. Anil, K. *Chopra Dynamics of Structures: Theory and Applications to Earthquake Engineering*; Pearson Education: Upper Saddle River, NJ, USA, 2013; ISBN 978-0-13-285803-8.
50. Montesinos López, O.A.; Montesinos López, A.; Crossa, J. Fundamentals of Artificial Neural Networks and Deep Learning. In *Multivariate Statistical Machine Learning Methods for Genomic Prediction*; Springer: Cham, Switzerland, 2022. [[CrossRef](#)]
51. Makridakis, S.; Spiliotis, E.; Assimakopoulos, V. Statistical and Machine Learning Forecasting Methods: Concerns and Ways Forward. *PLoS ONE* **2018**, *13*, e0194889. [[CrossRef](#)]
52. Shalev-Shwartz, S. *Shai Ben-David Understanding Machine Learning from Theory to Algorithms*; Cambridge University Press: Cambridge, UK, 2014. [[CrossRef](#)]
53. Edwin, R.; Mattias, S.; Guido, D.R. Macec—The Matlab Toolbox for Experimental and Operational Modal Analysis; 2021; Volume MACEC 3.4. Available online: <https://bwk.kuleuven.be/bwm/macec/macec.pdf> (accessed on 30 May 2023).
54. MIDAS IT Company Midas Civil Manuals and Tutorials. Available online: <https://globalsupport.midasuser.com> (accessed on 25 May 2023).
55. Pastor, M.; Binda, M.; Harčarik, T. Modal Assurance Criterion. *Procedia Eng.* **2012**, *48*, 543–548. [[CrossRef](#)]
56. Kennedy, J.; Eberhart, R. Particle Swarm Optimization. In Proceedings of the ICNN'95—International Conference on Neural Networks, Perth, Australia, 27 November–1 December 1995; Volume 4, pp. 1942–1948. [[CrossRef](#)]
57. Zeugmann, T.; Poupart, P.; Kennedy, J.; Jin, X.; Han, J.; Saitta, L.; Sebag, M.; Peters, J.; Bagnell, J.A.; Daelemans, W.; et al. Particle Swarm Optimization. In *Encyclopedia of Machine Learning*; Springer: Berlin, Germany, 2011; pp. 760–766. [[CrossRef](#)]

Disclaimer/Publisher's Note: The statements, opinions and data contained in all publications are solely those of the individual author(s) and contributor(s) and not of MDPI and/or the editor(s). MDPI and/or the editor(s) disclaim responsibility for any injury to people or property resulting from any ideas, methods, instructions or products referred to in the content.